12-2020

Fabrication and Flow Dynamics Analysis of Micromixer for Lab-on-a-Chip Devices

Md Fazlay Rubby

The University of Texas Rio Grande Valley

FABRICATION AND FLOW DYNAMICS ANALYSIS OF

MICROMIXER FOR LAB-ON-A-CHIP DEVICES

A Thesis

by

MD. FAZLAY RUBBY

Submitted to the Graduate College of
The University of Texas Rio Grande Valley
In partial fulfillment of the requirements for the degree of

MASTER OF SCIENCE

December 2020

Major Subject: Electrical Engineering

FABRICATION AND FLOW DYNAMICS ANALYSIS OF

MICROMIXER FOR LAB-ON-A-CHIP DEVICES

A Thesis

by

MD. FAZLAY RUBBY

COMMITTEE MEMBERS

Dr. Nazmul Islam
Chair of Committee

Dr. Samir Iqbal
Committee Member

Dr. Yong Zhou
Committee Member

December 2020

ABSTRACT

Rubby, Md Fazlay., <u>Fabrication and flow dynamics analysis of micromixer for lab-on-a-chip devices</u>. Master of Science (MS), December 2020, 80 pp., 2 tables, 54 figures, 21 references, 36 titles.

The miniaturized systems designed for lab-on-a-chip (LOC) technologies are generally implemented with a microscale mixer to provide intimate contact between the reagent molecules for interactions and chemical reactions. The exponential increase of research in microfabrication and microfluidic applications highlights the importance of understanding the theory and mechanism that governs mixing at the microscale level. In this study, the fabrication of an active and passive micromixer was discussed. The optimized state of art soft lithography and 3D printing were used as a microfabrication technique. The challenges at different fabrication steps were presented along with the modifications. Microelectrodes were integrated with the active microfluidic mixer to create an electrokinetic effect. The fluid flow field inside the micromixer was characterized by the Micro Particulate Image Velocimetry (Micro-PIV) system. Besides, numerical simulations were performed on 2D and 3D micromixers. Finally, results obtained in experiment and numerical simulations were analyzed to get better understanding of the micromixer design.

DEDICATION

The completion of my masters would not have been possible without the love and support of my family. My mother, Hasina Parvin, my father, Md Golam Mostafa, my wife, Fatema Hamim, and my father in law, RM Hafizur Rahman, wholeheartedly inspired, motivated, and supported me to accomplish this degree. Thank you for your love and patience.

ACKNOWLEDGEMENTS

I would first like to thank my thesis advisor Dr. Nazmul Islam. I would like to thank him for keeping me in place emotionally, whenever I ran into a trouble spot or had a question about my research or writing. He consistently allowed this paper to be my own work but steered me in the right the direction whenever he thought I needed it.

I would also like to acknowledge Dr. Samir Iqbal and Dr. Yong Zhou, for being the committee members of this thesis, and I am gratefully indebted to their very valuable inputs on this thesis. I also express my gratitude to Dr. Hasina Huq for letting me use her lab equipment.

Finally, I must express my very profound gratitude to my lab-mate Salman Parvez and to my wife Fatema Ha-mim for providing me with unfailing support and continuous encouragement throughout my years of study and through the process of researching and writing this thesis. This accomplishment would not have been possible without them. Thank you.

TABLE OF CONTENTS

LIST OF TABLES

x

LIST OF FIGURES

CHAPTER I

INTRODUCTION

Lab on a chip device overview

The rapid advances in microfabrication and nanofabrication combination with the

discovery of new materials have propelled the drive to develop new technological devices such

as lab-on-a-chip (LOC) and micro total analysis system (micro-TAS) to boost the affordable

healthcare system. These devices can yield diagnostic results at a patient home, a physician's

office, an ambulance, or a hospital. There would be no need for patients to travel long distances

to diagnostic centers and wait for days to obtain diagnostics lab results. A typical LOC device

and its components is presented in figure 1. Depending on the application such chips will contain

means of introducing a sample liquid and reagents, potentially reagent storage on chip, means of

mixing, separating, filtering of the fluids and structures for analytical readouts. Typically

structures for storage of used reagents and waste liquids also need to be provided. The most

crucial component of a LOC device is the micro-mixer. Because analytical results mostly depend

on the reagent mixing with the sample fluid. If the reagent mixing fails, it may alter the test

results. This research work represents the various design and the fabrication process of the

micromixer. The adoption of time and cost-effective fabrication methodologies is critical to the

future integration of these devices into mainstream biomedical applications. When large scale

fabrication is required these factors are likely to carry significance during the design process.
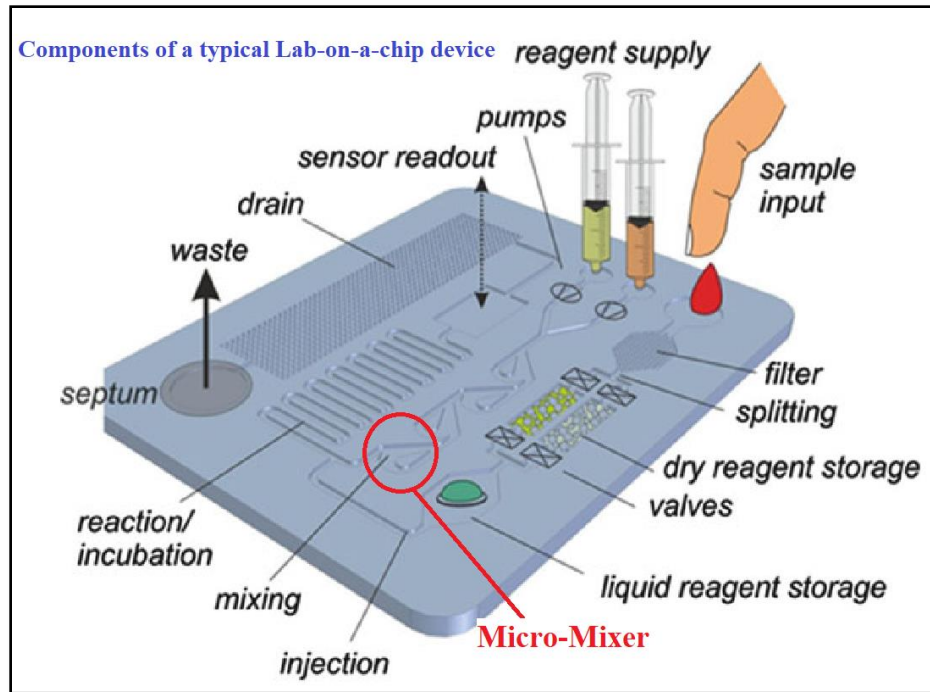
Figure 1: A typical LOC device and components. [1]

Micromixer overview

The fluidic structures in most LOC devices are very small in dimensions. The fluid flow is strictly laminar in small dimensions. This can be quantified by a dimensionless quantity known as the Reynolds number. This number is represented by the ratio of inertia to viscous forces. If this number is below 1,000-2,300 depending on the channel geometry, the flow is laminar. The typical Reynolds number for the LOC device is below 10. Laminar flow is considered as a disadvantageous property when diffusional mixing is required over short distances. For this, several concepts of micromixers have been developed which allow effecting mixing at low Reynolds number. There are two categories of micromixers. One is active mixers (which requires external actuation like electric or magnetic) and the other is passive mixers (which takes advantage of geometry).

2

Active micromixers depend on different external sources to disturb the fluids, increase the

contact area, or induce the chaotic advection, thus enhancing the mixing effect. The active

micromixers can be further categorized based on the external energy sources as electrical field

driven, pressure field driven, sound driven, magnetic field driven and thermal field driven. A

typical micromixer is presented in figure 2. Electric field is used to enhance the mixing effect in

the mixing chamber. Four electrodes are placed in the chamber wall to create the electroosmotic

effect.

Passive micromixers rely on the mass transport phenomena provided by molecular diffusion and

chaotic advection. These devices take the advantage of the channel geometry that increases the

surface area between the different fluids and decreases the diffusion path. The chaotic advection

is enhanced by modifying the channel design. This chaotic advection manipulates the laminar flow

inside the mixing chamber. The modified flow pattern must follow a shorter diffusion path that

improves the mixing velocity. The channel geometry of a passive micromixer is presented in figure

3.
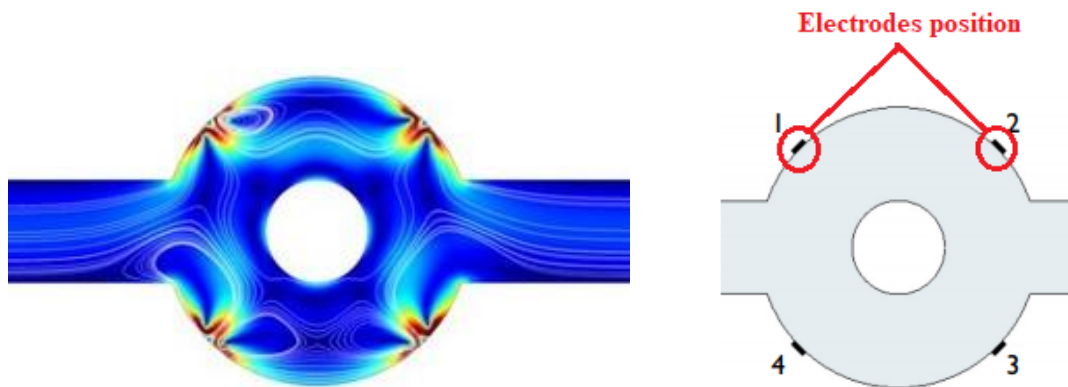
Figure 2: A typical active micromixer (electroosmotic). [2]
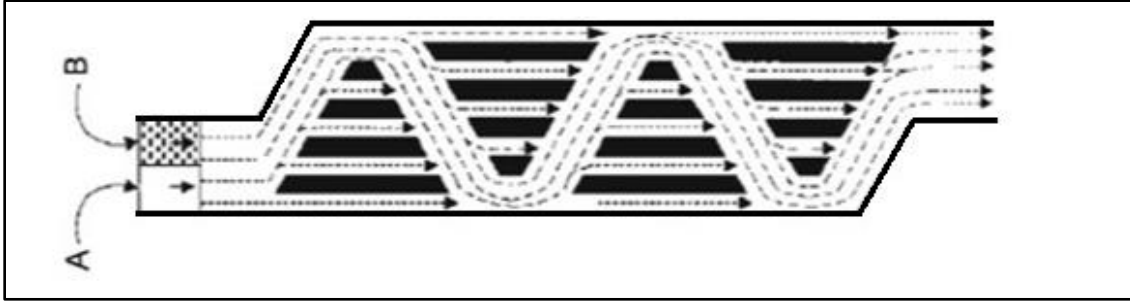
Figure 3: The internal geometry of a passive micromixer. [3]

Electrokinetic fluid manipulation

The manipulation of colloidal particles and fluids in microsystems has many existing and potential applications. Among the most promising techniques to handle small objects at the micrometer scale are those that employ electrical forces, which have the advantages of voltage-based control and dominance over other forces. The latter is a clear example of the scaling laws of physical systems: in the range above a few millimeters the electrical forces are rather ineffective, but in the micrometer (and submicrometric) scale the electrical forces dominate. There are several electroosmotic that can affect microscale flows. Among those, the electroosmotic force is used in this experiment to manipulate microscale flows.

Electric double layer and Debye length

When an electric field is applied in an electrolytic solution with dissolved ions and moderate conductive, then the counter ions of the electrolyte can easily move to the interface of the electrode. For example, in figure 4, when ionic liquid meets a negative surface, the positive charges of the liquid are attracted to the solid surface. At the very interface of the solid surface, these positive charges are strictly bound to the negative charges and these positive charges form an immobile layer which is known as the stern/ Helmholtz layer. There are also some negative

charges which are attracted to the stern layer. But the number of positive charges will be greater

than the negative charges in this region. So, this region will have a net positive charge. This

region is called the electric double layer (EDL). This is also known as the diffuse layer. There

will be an equal number of positive and negative charges beyond this region.

Now, we will look at the potential from the solid surface to the bulk of the liquid in Y direction.

In figure 4, the potential Phi is going to vary from the solid surface to the bulk. The potential in

the stern layer is known as the zeta potential. This zeta potential depends on the solid surface as

well as the liquid. The potential becomes zero in the bulk. The distance between the stern layer

and the diffuse layer is known as lambda. It is called the Debye length (λ_D). The typical value of

zeta potential (ξ) for glass is -88 and for PDMS is -110 to -68. It is very important for

electroosmotic flow.
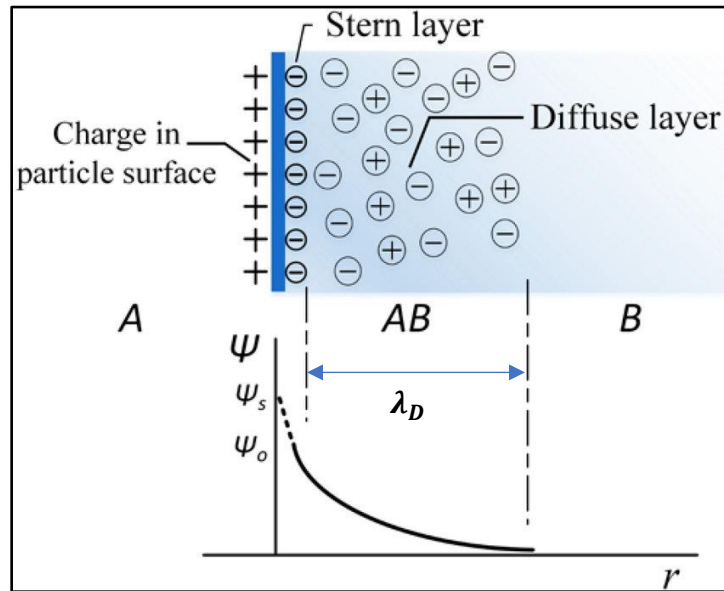
Figure 4: Electric double layer and Debye length. [4]

The governing equation for electroosmotic flow

Fluid manipulation is a very critical issue in micromixer and micropump because of

capillary action in microscale. Fluid flow due to the electric field between two parallel plates will

be discussed in this section. In figure 5, There are two positively charged parallel plates. Ionic liquids occupy the place between the parallel plates. There is a positive electric terminal on the right side and a negative terminal on the left side of the channel. Since the plate surface is positively charged, there will be a negatively charged region in the electric double layer near the plates. So, when an external electric field is applied in two terminals, these negative charges will migrate towards the positive terminal. Thus, it will create a velocity in the positive X direction.
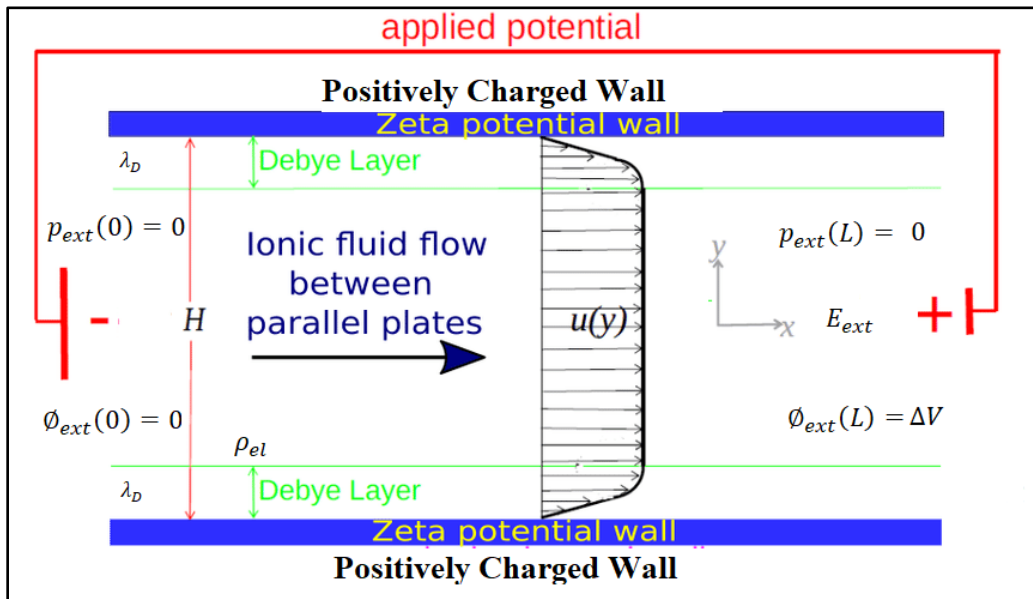
Figure 5: Electroosmotic flow between parallel plate channels

The velocity in the parallel plate channel is expressed by the famous Naiver-Stokes equation. The equation is given below,

$$\rho_f \left(\frac{\partial \vec{V}}{\partial t} + (\vec{V}.\nabla)\vec{V} \right) = -\nabla P_{ext} + \eta \Delta^2 \vec{V} - \rho_{el} \nabla \emptyset_{ext} \qquad \text{(Eq 1)}$$

Here,

ρ_f = the fluid mass density,

V = the flow velocity,

P_{ext} = the external pressure,

$\rho_{el}\nabla\emptyset_{ext}$= the body force due to electric potential,

ρ_{el} = the electrical charge density and

$\nabla\emptyset_{ext}$= the potential distribution.

In Naiver-Stokes equations, the first and second terms of the left-hand account for the transient and advective contribution in fluid flow, while the first and second terms on the right-hand side are related to pressure and viscous forces. In most micro/nanofluidic systems, the advective term is much smaller than the viscous term due to the small length scale and ultra-low flow velocity. To get the velocity expression from the Naiver-Stokes equation following assumption was taken.

1. Steady and uniform flow parallel plate channel (Length= L) is considered. Velocity only varies in the Y direction. So, velocity distribution, $\vec{V}(r) = U(y)\,e_x$ (Eq 2)

2. Charged walls are located at, y= ±h/2   (Eq 3)

3. The external pressure gradient is zero.

So, $p_{ext}(0) = 0, \; p_{ext}(L) = 0.$ (Eq 4)

4. The external electric field is in negative X direction.

So, electric field distribution, $\vec{E} = -Ee_x$.   (Eq 5)

Electric potential distribution, $\nabla\emptyset(r) = -E = Ee_x$.   (Eq 6)

Maxwell's equation for electric charge density, $\rho_{el} = -\varepsilon\nabla^2\emptyset(r)$.   (Eq 7)

Here, ε is defined by fluid's permittivity.

5. The external electric field does not change the charge density.

Now, the X- component of the Naiver-Stokes equation can be written in the following form.

$$\rho_f\left(\frac{\partial U}{\partial t} + (U.\nabla)U\right) = -\frac{\partial P}{\partial x} + \eta\Delta^2 U - \rho_{el}\nabla\emptyset_{ext} \qquad \text{(Eq 8)}$$

After applying the assumptions stated earlier, the terms of the equation can be evaluated as below

For steady flow, $\frac{\partial U}{\partial t} = 0$ (Eq 9)

For uniform flow, $(U.\nabla) = 0$ (Eq 10)

For no external pressure, $-\frac{\partial P}{\partial x} = 0$ (Eq 11)

So, the equation becomes, $\eta \frac{\partial^2 U}{\partial^2 Y} + \varepsilon \left(\frac{\partial^2 \emptyset(Y)}{\partial^2 Y}\right) E = 0$ (Eq 12)

After integrating both sides of the equation, it will be written as below

$$\eta U(Y) = \varepsilon \emptyset(Y) E + C_1 Y + C_2$$ (Eq 13)

The equation will be evaluated based on the boundary condition stated below,

1. No slip condition, $U\left(\mp\frac{h}{2}\right) = 0$ (Eq 14)

2. When, $Y \to \infty, \frac{\partial U}{\partial Y} = 0$ (Eq 15)

   To satisfy this condition, $C_1 = 0$ (Eq 16)

3. At the wall, $\emptyset(Y) = \xi$ (Zeta potential) (Eq 17)

So, the equation becomes, $U(Y) = [\xi - \phi(Y)]\frac{\varepsilon E}{\eta}$ (Eq 18)

Now applying the Debye-Huckel limit ($\lambda_D \ll h$) in the equation.

$$U(Y) \approx U_e = \frac{\varepsilon \xi E}{\eta}$$ (Eq 19)

It is the expression for the velocity profile of ideal electroosmotic velocity. This velocity is directly proportional to zeta potential, electric field, and permittivity of the fluid. It is inversely proportional to the viscosity of the liquid. This equation will be used as a boundary condition for the numerical simulation of the micromixer.

CHAPTER II

LITERATURE REVIEW

Lab on a chip for biomedical applications and micro laboratories for biochemical applications usually require rapid mixing of a different fluid stream. Fluid flows in a highly ordered laminar fashion without the presence of any turbulence at the microscale. This makes diffusion the primary mechanism for macromixing. Diffusional mixing for small molecules can occur in a matter of seconds over small distances of micrometers. But for large molecules like peptides, proteins and high molecular weight molecules can take long equilibration times from minutes to hours over small distances. Microscale mixing devices are categorized into two types. One is passive mixers that use geometrical stirring and the other is active mixers that use moving parts or external forces like pressure or electric field. Passive mixers often require long mixing channels because the different fluids run in parallel. A novel in-plane passive microfluidic mixer was designed by Hong et.al. [5]. A Tesla structured passive micromixer was proposed which could be worked at the flow rate of 100 µl/min and a pressure drop of 10 KPa. The dimension of the mixing zone was 2 cm. this is very large compare for an active micromixer. Another way to improve the efficiency of the micromixer is to use an active mixer with moving parts. But moving parts in an active micromixer are very fragile at the microscale. One alternative is to use the electric field to do the mixing. When an electric field (AC/DC) is applied to a fluid, the interactions between electrolyte-electrode microsystem were clearly described by J. Wu [6].

In her research Dr. Wu showed that at low-frequency capacitive impedance was dominated over resistive impedance, which causes AC-electroosmosis. This generates fluid motion near the electrode surface. If an electric field is applied perpendicular to the fluid flow it will create a mixing effect because of electroosmosis. This mechanism was used by many researchers to build an active micromixer. Numerical simulation of an electroosmotic micromixer was done by Chen et.al. [7]. A time-dependent electric field was applied to the low Reynolds number flow. An incompressible Naiver stokes equation was solved using an electroosmotic slip boundary condition. It was found that if the electric field assumed as a quasi-steady then the particle traces showed folding and stretching of material lines. It created a chaotic mixing environment in the channel. Numerical simulation of biofluid mixing as a non-Newtonian fluid was carried out by Hadigol et.al. [8]. They found that the mixing efficiency decreases as the Reynold number increases for non-Newtonian fluid when a DC-electric field is applied in the electrodes. Higher mixing efficiency was found for a wide range of Reynolds number rather than the Newtonian fluids. An experimental electroosmotic micromixer was fabricated and tested by some researchers. A ring electroosmotic micromixer was fabricated by Zhang et.al. [9] using bulk micromachining technology on top of an SOI wafer. A microchannel of 25 microns wide and 50 microns deep was fabricated using two steps photolithography. The microelectrodes were characterized by Focus Ion Beam System. A micro-PIV system was used to test experimental flow-field analysis. A rapid experimental micromixer was designed by Sasaki et.al. [10]. A pair of the coplanar zigzag electrode was fabricated using a wet etching technique configured in parallel to the channel. Dilution of di water and dye was observed to compare the mixing performance. The channel width was 120 µm. Rapid mixing was observed up to 12 mm/s inlet velocity. The mixing time was 0.18 s which was 20 times faster than traditional diffusional

mixing. To improve the mixing efficiency some researchers tried to change the channel dimensions along with the applied voltage. Sometimes dimensions of the charged surface were changed to improve the mixing efficiency. Such effort was carried out by Ahmed and Kim [11] in their recent work of the parametric study of micromixer. They did a parametric analysis of the micromixer by varying channel height, width, and size of the charged surface. They found that using two heterogenous charge surfaces will increase the mixing efficiency of the mixer. Another attempt of increasing mixing efficiency by introducing asymmetric lateral structure was done by Zhou et. al. [12]. By introducing asymmetry in the channel, they found that it showed enhanced disturbance at low voltage. The research group observed enhanced mixing compared to traditional symmetric ring type structure. Many researchers have done analyses separately for numerical and experimental analyses. A few works were done combining experimental and numerical analysis on micromixers. One recent approach was taken by Zhang et. al. [13] using asymmetrical floating electrodes. Simple planar electrodes were made using ITO coated glass to test the mixing. The maximum mixing efficiency was found 94.7% with 3.2 mm mixing length under a sinusoidal peak voltage of 14 V and a frequency of 400 Hz at a flow rate of 1500 µm/s. Numerical and experimental results showed similar patterned results. Another recent work was done by Azam Usefian and Morteza Bayareh [14]. Two half circle electrodes were made by gold nanoparticles which were incorporated with the microchip made of PDMS. Both AC and DC voltage were applied in the electrode experimentally along with the numerical simulation. The result showed that the mixing performance can be controlled by the applied voltage and the inlet velocity of the fluids. Mixing performance was improved by enhancing the applied voltage and decreasing the inlet velocity.

11

LOC is one of the major application areas of the multifunctional fluid and bioparticle micromixer. LOC is the future of human disease diagnosis and treatment. As it requires less sample, less time, and less reagent to detect disease. The major drawback of the LOC device is the incubation time. The incubation time was reduced by using AC electrokinetic method in an immunoassay lab-chip by Yang et.al. [15]. In their work, they applied AC signals over interdigitated electrode arrays on the microchannel bottom. This generated an ACET micropump, which was used to deliver the reagent and analyte to the inspection site. This ultimately shortened the incubation time from 30 minutes to 1 minute. Another LOC prototype for microorganism detection and manipulation was designed by Medoro et.al. [16]. They used a printed circuit board (PCB) with the enclosed dielectrophoretic cages to trap, concentrate, and quantify polystyrene micro-beads. They effectively manipulated and detected particles without the help of an external optical component. By integrating DEP in the process, particle concentration increased on the chip more than three orders of magnitude boosting the detection accuracy. The surface-based biosensor is another major area where multifunctional fluid and bioparticle manipulators could play a vital role by improving detection time, sample amplification, and transportation. Conventional micro-organisms detection techniques completely depend on bacteria incubation on nutrient media and cell culturing of viruses. It takes several days or weeks for this process to complete. It increases the detection time of bioparticles. One way to reduce the detection time is to use AC electrokinetic fluid manipulation. This will increase the concentration of the bioparticles in the sensor surface by overcoming the diffusion problems. ACEO trapping and detection of bioparticles were done by J. Wu et.al. [17]. In this work, they discovered that by using parallel microelectrodes separated by 40 µm, bioparticles were trapped on the electrode surface by AC electroosmotic effect. Then, they detected the

12

bioparticles using impedance spectroscopy. It was observed that the integration of AC electroosmosis with impedance measurement improved the sensitivity and reduced the detection time of bacteria in the solution. Another work was done by Tomkins et.al. [18] presenting a biosensor combination of cantilever and microelectrodes for enhanced pathogen detection. Quadrupole micro-electrodes were fabricated on top of a micro-cantilever to detect the presence of E. coli. bacteria. The microelectrodes pattern creates a dielectrophoretic effect that trapped the bacteria on the cantilever surface. This helped the cantilever to detect E. coli. bacteria without the need for cultivation. This reduced the total detection time of the sensor. Recently, AC electrokinetic mechanism is greatly used in nanoparticle-based plasmonic optical biosensing. One related work was done by Song et.al. [19]. They detected cytokine biomarkers using AuNR biosensor. AC electroosmosis was used in the sensor to enhance performance. They were able to detect cytokine biomarkers within 5-15 minutes from diluted human serum. Point of care medical diagnosis and LOC devices often require biological cell transportation, separation, mixing with reagents, and trapping performed in a single device.

CHAPTER III

DEVICE FABRICATION

Fabrication using the soft-lithography method

Soft lithography was used in this experiment as a fabrication technique for making a microfluidic mixer. It is done in two steps. First, the SU-8 mold is prepared on top of a silicon wafer. Second, the pattern is transferred to the Polydimethylsiloxane (PDMS) using a stamping process. Normally, it is viewed as an extension of photolithography.

SU-8 mold fabrication

The mold fabrication process was taken from manufacturer **Microchem**. It is followed by manufacturing guidelines (www.microchem.com). The complete process flow diagram is presented in figure 6. SU-8 2025 is used as a negative photoresist. It has several advantages over other photoresist materials. It has improved coating quality and increases process throughput. The film thickness can be achieved up to 200 microns with a single coat.

1)   Substrate Preparation. Four inch pure silicon wafer was used as a substrate. Normally single crystal polished silicon wafer was used for MEMS and microfluidics application. It is usually cleaned with a piranha wet etch (using H_2SO_4 & H_2O_2) followed by a de-ionized water rinse. But we don't have any piranha solution in our lab. We follow the following steps to prepare the substrate, 1) substrate is cleaned with acetone, 2) it is dried with clean air, 3) then it is heated for 10 mins. At 120ºC in the hotplate for better sticking of photoresist.

14
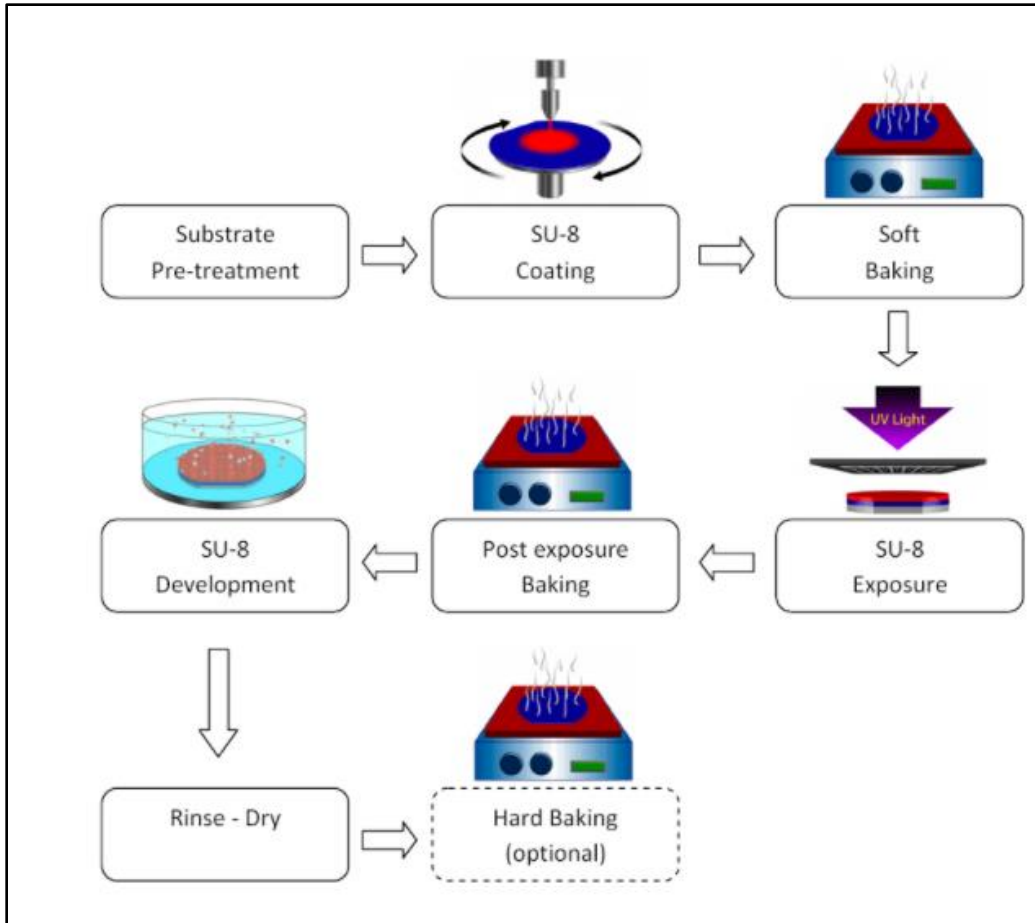
Figure 6: SU-8 mold fabrication steps

2) **Photoresist Coating.** Photoresist coating time and rotation speeds depend on film thickness. To get the optimal thickness, the following graph was followed. It is provided by the manufacturer. Based on the graphs (Expected thickness 40 microns), the following guidelines are followed during spin coating. 1)1ml of photoresist is used for 1 inch of substrate diameter, 2) Spin at 500 rpm for 5-10 seconds with the acceleration of 100 rpm/second, 3)Spin at 2000 rpm for 30 seconds with the acceleration of 300 rpm/second.

3) **Edge Bed Removal.** It is done for better mask alignment and improved resolution. This step is skipped for the current trial. Because it will not create any effect on the experimental results.

Figure 7: a) Spin coater, b) SU-8 negative photoresist.

4)   Soft Bake. Soft baking time depends on the film thickness. The manufacturer table is used to determine the baking time. It is usually depends on the thickness of the photoresist coatings. The expected thickness for the current coating was 40 microns. In this condition, the wafer along with the photoresist was heated for three minutes at 65°C and five minutes at 95°C.

5)   UV Exposure. The most important part of soft-lithography is UV exposure. Two things are needed to do the UV exposing. One is the UV source and another one is the mask to obstruct the UV. The optimal light wavelength for SU-8 exposure is 365nm. To fulfill the UV wavelength requirement a UV flashlight (Model-UV301D-plus) was bought from Amazon. It is commercially used by the UV glue curing professional. The UV exposure set-up is highlighted in figure 8(b). The maximum light emission energy was 200mW/cm^2. It depends on the distance the exposing object is kept. The exposure energy also depends on the photoresist thickness. From manufacturer guidelines, the optimum exposure energy for 40 microns is 150mJ/cm^2. The exposure time is calculated from the formula, exposure time = (required exposure energy/ the lamp emission energy). Another important thing for UV exposing is the mask. It is allowed the UV light only in the desired exposing area. Normally, it is made of a glass plate. But we don't

have that facility in our lab. It is printed on transparent plastic paper using a high resolution (1200dpi) office printer. First, the pattern was drawn using Autocad software. Then, it was printed. The mask is illustrated in figure 8(a).
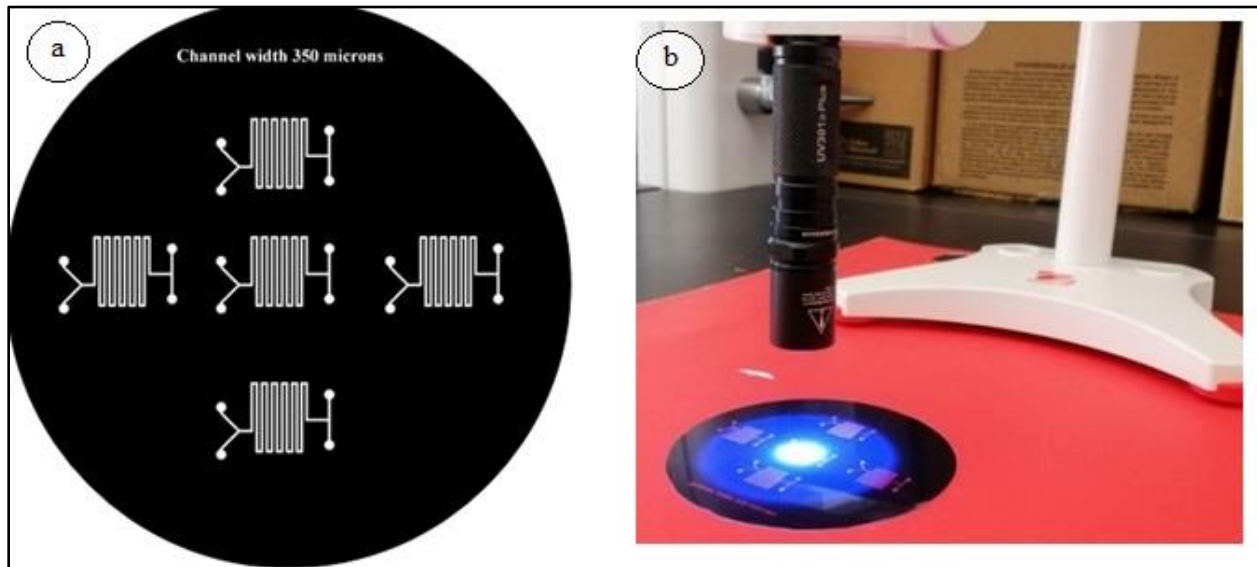
Figure 8:a) Printed mask in the transparent plastic paper, b) UV exposure set-up.

6)   **Post exposure bake.** After exposure, the substrate should directly move to the hot plate for post exposure bake. The temperature and the time being followed by the manufacturer's guidelines. It depends on the photoresist thickness. For 40 microns thickness, the substrate was heated at 65°C for one minute and at 95°C for five minutes.

7)   **Development.** PGMEA (Propylene Glycol Monomethyl Ether Acetate) is used as a SU-8 photoresist developer. The developing time is selected from the manufacturer guidelines. It was developed for five minutes.

8)   **Rinse and dry.** To remove developer solution from the substrate surface following rinse and dry procedure was followed. 1) The substrate was sprayed and washed with fresh developer

solution for 10 seconds, 2) then it was sprayed and washed with Isopropyl Alcohol for 10 seconds, 3) finally, the substrate is dried with pressurized air.

9) **Hard bake.** From the manufacturer's recommendation, it is suggested that it should be baked at 150°C for two minutes. It applies to all photoresist thickness. After following the above steps, the final SU-8 mold was obtained. The final SU-8 mold along with the microscopic view is illustrated in figure 9(a), and 9(b).
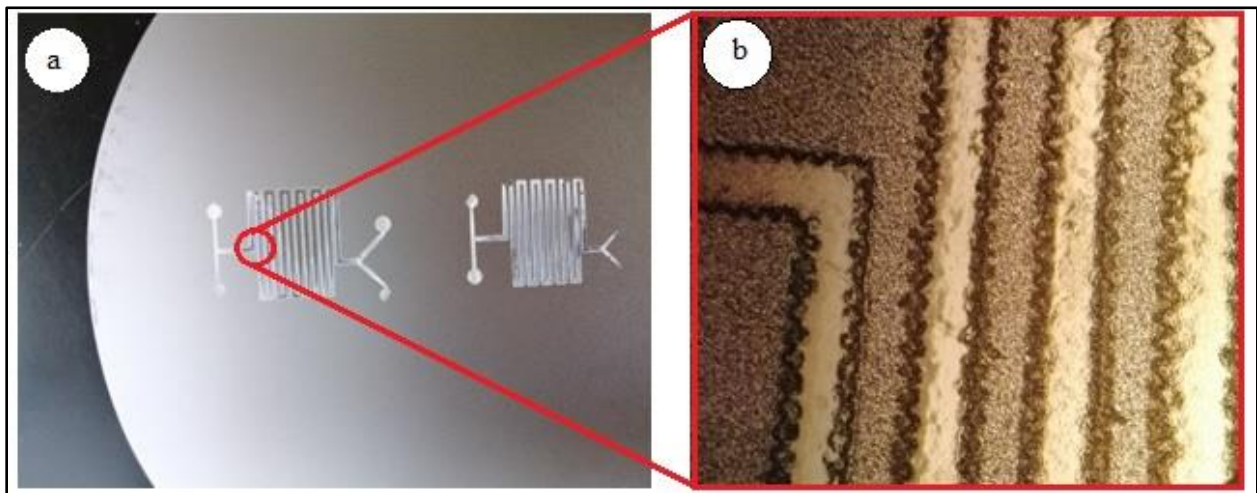
Figure 9: a) Final SU-8 mold on top of a silicon wafer, b) microscopic view of the mold.

PDMS replication of the SU-8 mold

The PDMS is a polymer widely used in microfluidics to make devices such as lab on a chip. The replication process is mainly divided into 8 steps.

1. The preparation of the mold with the silanization

2. The scaling and mixing of the PDMS and the curing agent

3. The degassing to remove bubbles

4. The PDMS pouring on the mold

5. The PDMS baking

6. The PDMS peeling off the mold

7. The PDMS cutting and piercing

8. The PDMS bonding

The steps of the PDMS replication is discussed in detail below.

1.   **Silanization of SU-8 mold.** This process is intended to produce passivation of the surfaces to aid release from PDMS and prevent the PDMS from adhering to the master. The procedure is given below. 1) The SU-8 mold was cleaned with compressed air, 2) Inside the fume hood, two drops (use plastic pipette) of the salinizing agent was dropped in a petri dish, 3) The petri dish containing the silanizing agent was covered with the wafer and kept in the vacuum desiccator, 4) The wafer was kept on the hotplate in the fume hood 150ºC for 10 mins to cure and evaporate the excessive silane. The SU-8 mold after silanization is illustrated in figure 10.
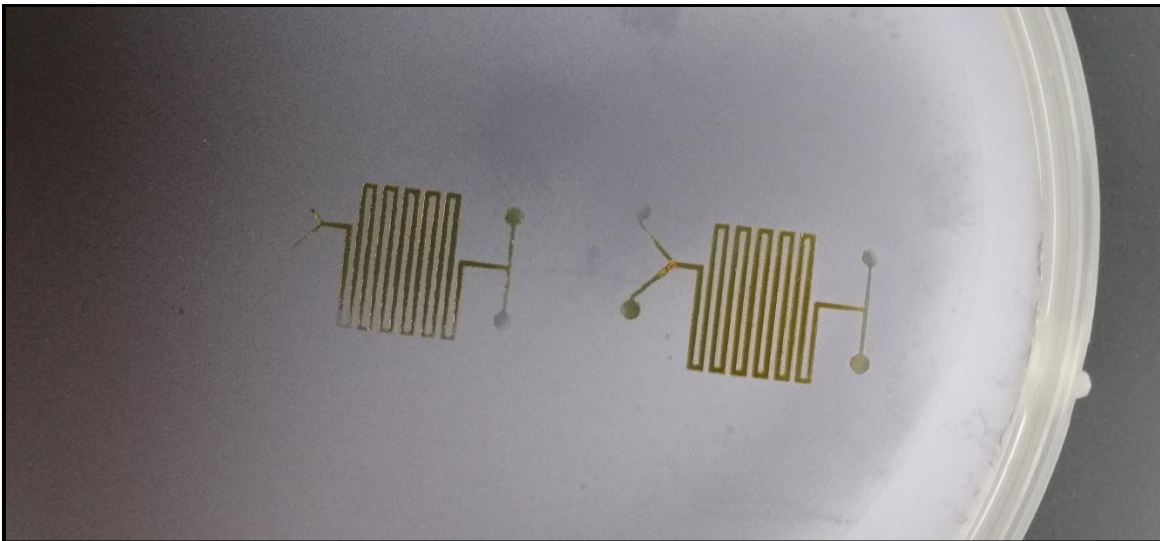
Figure 10: SU-8 mold after silanization. The color was slightly yellowish.

2.   **The mixing of PDMS and curing agent.** Once mold is ready, the PDMS can be prepared. PDMS is the name of the polymer. To make it harder a curing agent is needed to add. The most used PDMS is clearly the Sylgard 184. For this PDMS the usual ratio between the curing agent and the PDMS is 1:10 (weight). It was about 44gm of PDMS needed for a 4-inch wafer to achieve a thickness of 5mm. To prepare my PDMS, I followed the recipe below. 1) Weight of the PDMS base (40gm), 2) Weight of the curing agent (4gm), 3)Mixed it strongly using an automatic mixer at 300 rpm.

3.   **The degassing to remove bubbles.** The mixture was filled with bubbles due to mixing. These bubbles must be removed because if not they will be trapped inside the PDMS chip. There are different ways to degas the PDMS mix. I used a desiccator for this purpose. The mix was kept inside the desiccator. A vacuum pump was used to remove the air inside the desiccator. Once the bubbles were removed, the PDMS mix was taken out carefully.

4.   **The PDMS pouring on the mold.** The SU-8 mold was cleaned using clean compressed air to remove all dust and particulates from the mold surface. Once the PDMS mix was degassed, it was poured on the SU-8 mold. A round arrangement was made around the SU-8 mold wafer using aluminum foil.
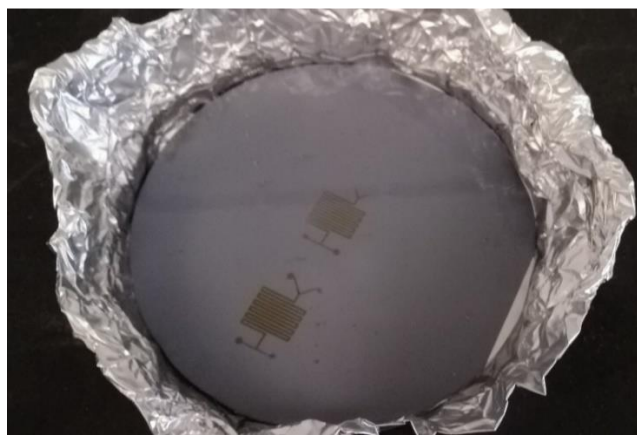
Figure 11: SU-8 mold and PDMS mix in an aluminum foil cup.

5. **The PDMS baking.** Once the PDMS and the curing agent are mixed, the cross linkage

has begun but alone it will take around 24 hours to get a solid enough device. That is why the

mold and the PDMS must be baked. The time and temperature of the baking vary depending on

the laboratory and the user, as well as the tools used. In our lab, we used a hot plate for PDMS

baking. I kept it on the hot plate at 100°C for 35 minutes.

6. **The PDMS peeling off from the mold.** Once the mold was cooled down to room

temperature, the PDMS layer was peeled off from the mold surface using a scalpel and a paper

cutter.
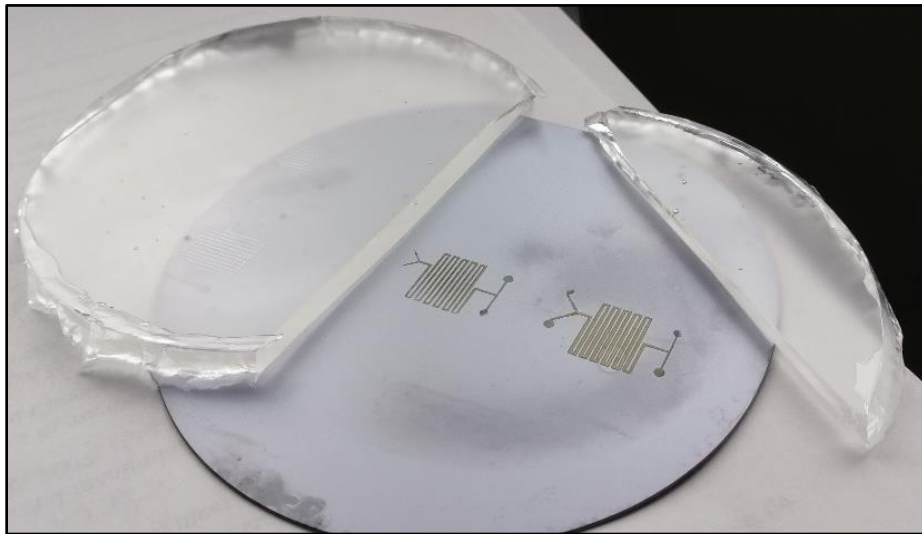
Figure 12: PDMS peeling off and cutting.

7. **The PDMS cutting and piercing.** After peeling off, the PDMS was cut in the shape of a

microscopic slide. Because it will be used on top of a microscopic slide. Then, a punch was used

to create an inlet and outlet hole in the microfluidic channel. The diameter of the punch was

2mm. The replicated PDMS channel is illustrated in figure 13(a).

8. **The PDMS bonding.** The last step is to bond the PDMS device and the glass slide. The

PDMS can be bound on another piece of PDMS or glass but the protocol is the same. Before

anything, each part must be well cleaned to remove any dust or particles from the surface. To bond the PDMS the surface needs to be activated, transforming the Si-CH3 function of the PDMS to a Si-OH, and when it will be pressed against the same function it will create a strong and permanent Si-O-Si link. To do so the most used tool is a plasma cleaner working with O2 or air.
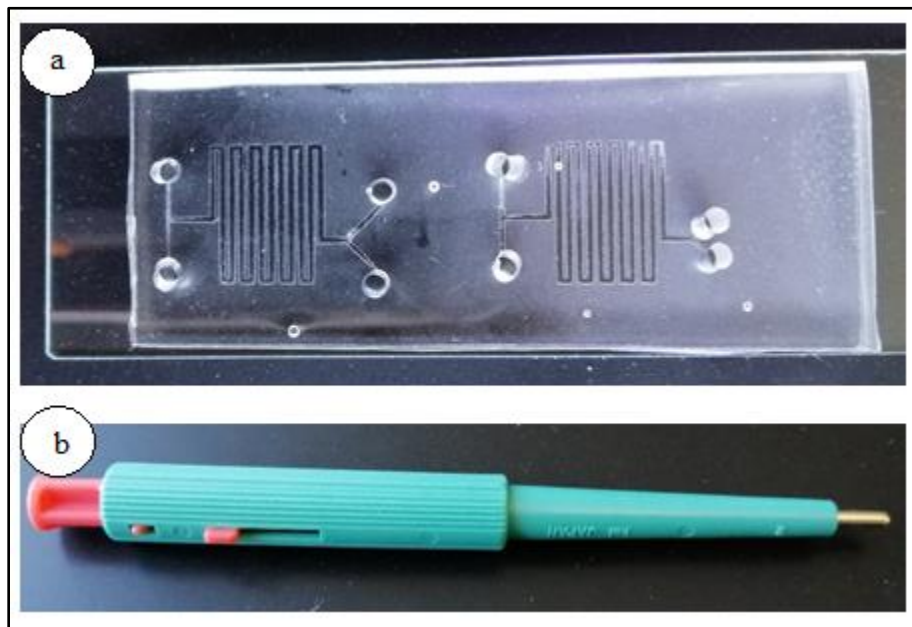
Figure 13: a) The PDMS microchannel after cutting and piercing, b) The punch is used for Piercing.

Fabrication using 3D printing

3D printing has the potential to revolutionize the fabrication method of microfluidics. The traditional soft lithography method has some drawbacks. It requires several steps to get the final product. It also requires complex process equipment, different raw materials, and a significant amount of time. More importantly, this method lacks the ability to create complex 3D structures.

22

On the other hand, 3D printing can create complex three-dimensional structures. It will lead the opportunity to create innovative microfluidic structures which is not possible using existing approaches. There are several 3D printing techniques used by researchers to create microfluidic structures. They are, 1) inkjet (i3DP) printing, 2) Stereolithography (SLA), 3) two photon polymerizations (2PP), and 4) extrusion printing. In this study, stereolithography was used for 3D printing.

Stereolithography (SLA) 3D printing overview

SLA 3D printing has become vastly popular because of its ability to produce high-accuracy, isotropic, watertight parts in a range of advanced materials with fine features and smooth surface finish. It is a method and apparatus for making solid objects by successively printing thin layers of a UV curable material one on top of the other. Objects are built in a layer-by-layer manner by spatially controlled photopolymerization of a liquid resin which is performed with either a scanning laser or a digital light projector. The bath configuration of a classical SLA set-up has been illustrated in figure 14. A UV beam traces a 2D cross section onto a support platform submerged in a tank of photoactive resin. This photoactive resin undergoes a polymerization reaction upon UV illumination. After completion of the 2D cross section, the platform is lowered further into the resin and the UV beam begins the addition of the next layer. The product is ready after the completion of the final layer. The 3D fabrication of the microfluidic mixer was completed in the following steps.

1.   **Design of 3D microfluidic Channel.** The 3D geometry of the microfluidic mixer was designed using AutoCAD software. The drawing file is exported as a 3D printable file format (STL). The 3D drawing of the microfluidic mixer is presented in figure 15.
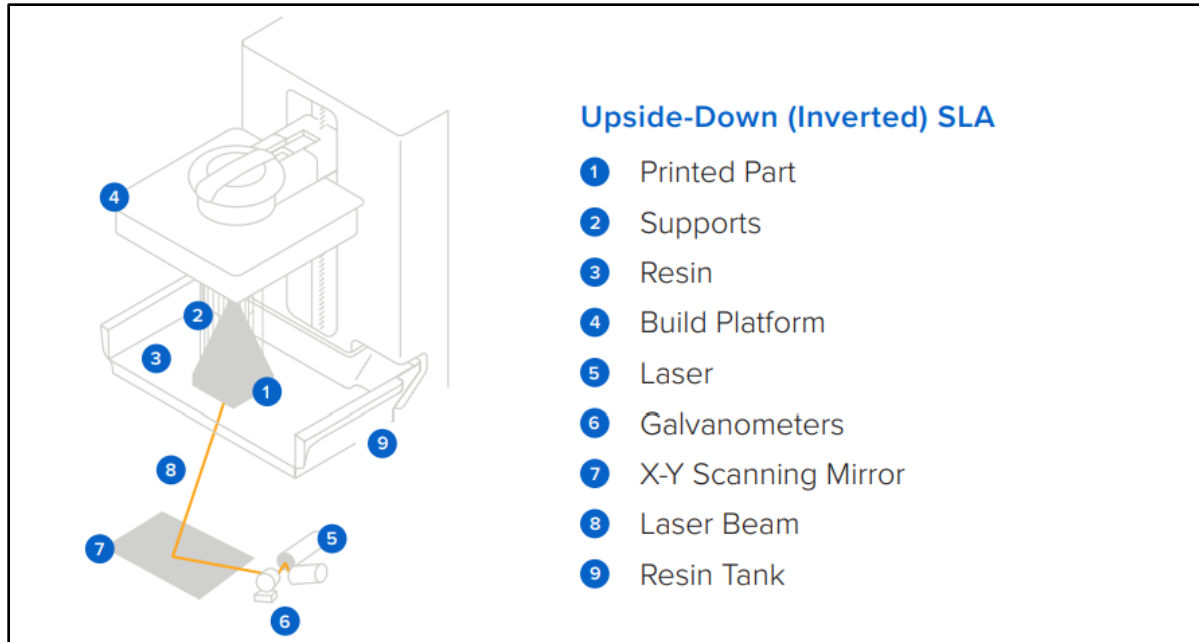
Figure 14: A graphic representation of basic mechanism of the SLA 3D printing. [20]

2.   **Slicing using CHITUBOX software.** The 3D model of the microfluidic mixer is sliced using CHITUBOX software. The different features can be added to this software to make it a stable 3D printing object. Because it will be printed in the 3D printer in a layer by layer manner. The setting of each layer like the amount of UV light, exposure time, printing time, amount of materials, and cost of the printing can be adjusted in this software. It is very useful to make low-cost microfluidic objects. Examples of slicing are given in figure 16.

3.   **3D printing.** ELEGOO Mars UV Photocuring LCD 3D printer (Figure 27) was used for 3D printing purposes. The 3D drawing file after processed by CHITUBOX software was fed into the printer by a pen drive. Before starting the printing process, the standard photocuring liquid was supplied to the printing chamber. The amount was adjusted depending on the volume of the 3D printed object. After post-processing, the final product is achieved.
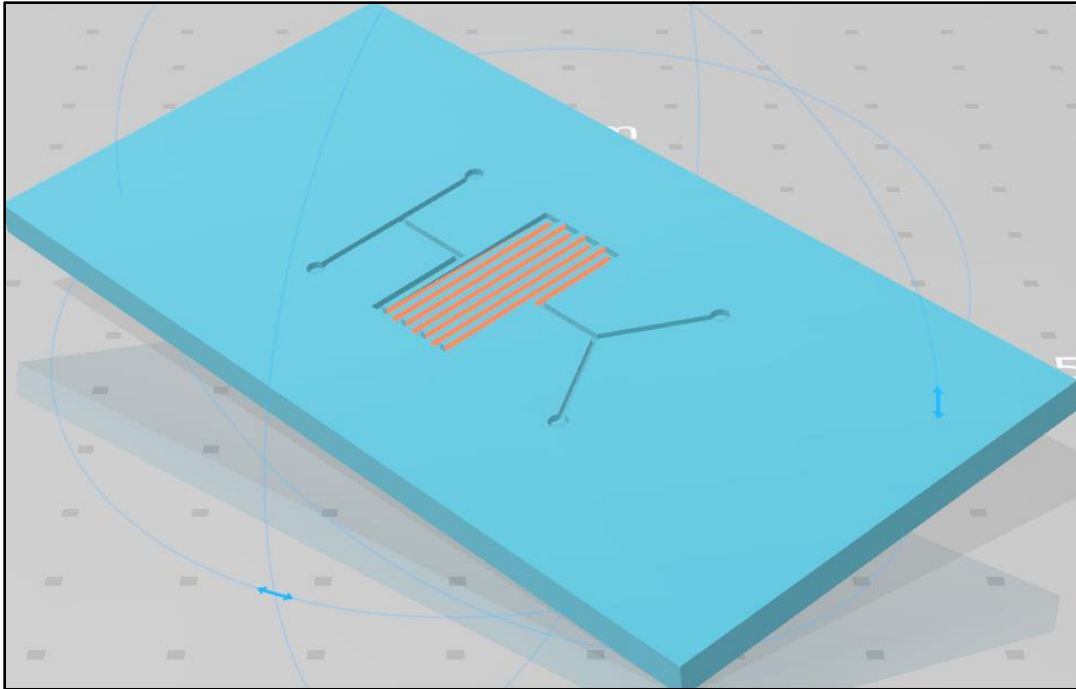
Figure 15: 3D design of the microfluidic mixer.

4. **Post-processing.** Once the printing is completed, parts require rinsing in isopropyl alcohol (IPA) to remove any uncured resin from their surface. After rinsed parts dry, some materials require Post-curing, a process that helps parts to reach their highest possible strength and stability.

5. **Integration with PDMS slice.** To complete the fabrication of the microfluidic mixer the 3D printed part was combined with a PDMS slice. The PDMS slice confined the microfluidic channel so that liquid can flow inside the channel without any leakage. The PDMS slice is stamped on top of the 3D printed part. Inlet and outlet opening in the PDMS slice were created using a biopsy punch. The PDMS slice fabrication was described in the previous section.
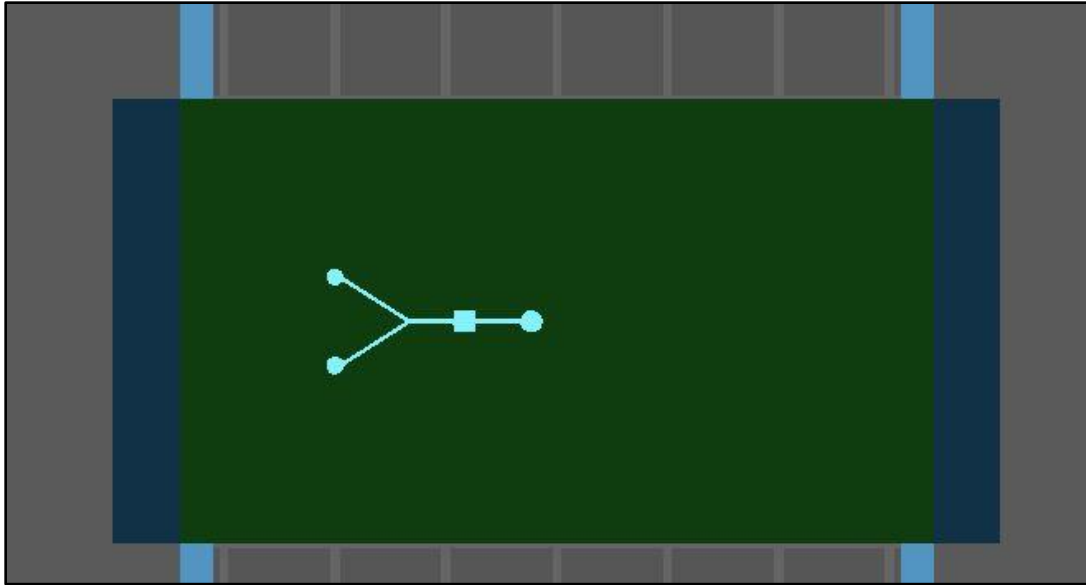
Figure 16:Slicing of the 3D objects before printing.

Figure 17: a) ELEGOO Mars UV Photocuring LCD 3D printer, b) Photopolymer resin.

Planar fabrication of micro-electrodes

Planar electrodes were fabricated on top of a silicon wafer using the sputtering system. Total fabrication process was completed in three steps. They are 1) masking, 2) Gold sputtering, and 3) mask removal.

1.   **Masking.** To sputter the electrode on top of the wafer a mask was required. Two types of the mask were used for electrodes fabrication. One type of mask was fabricated by the house 3d laser cutter. Aluminum foil was used for electrodes patterning for this type of mask. Another type of mask was created using masking tape. It is easy to fabricate compared to an aluminum mask. But the aluminum mask is used to get the smooth pattern and the smaller size electrodes.
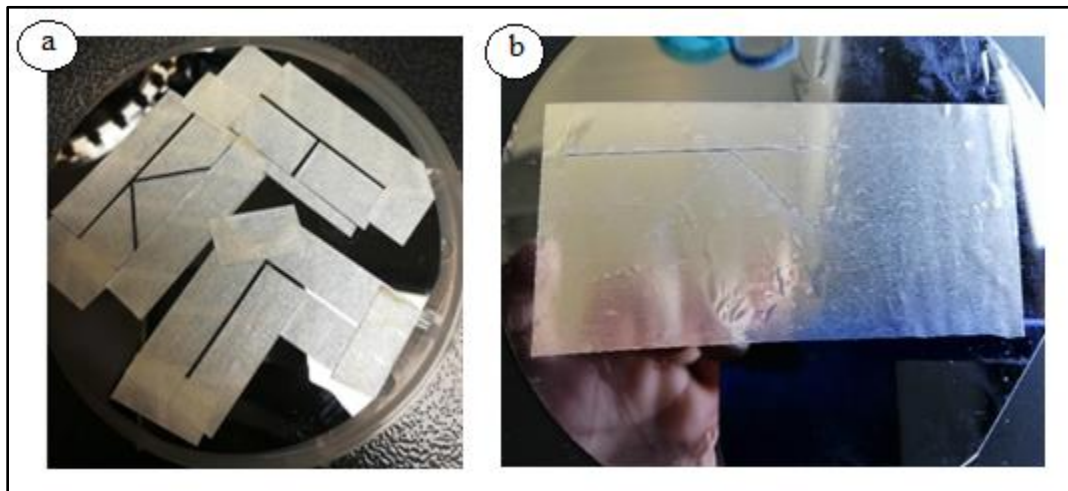
Figure 18: a) Masking of the wafer using masking tape, b) Masking of the wafer using Aluminum foil.

2.   **Gold sputtering.** Two-layer combination of Titanium and Gold were sputtered. The titanium (30nm) layer was used as an adhesive layer and the Gold (120nm) layer was used as an

electrode. Gold was deposited on the substrate by dc magnetron sputtering machine (AJA ATC

Orion 5 Sputtering System). First, the silicon substrate was cleansed with isopropyl alcohol,

acetone, and deionized water and then dried with compressed air. The sputtering system was

vacuumed to a pressure of 6.8×10^{-6} Torr before starting the deposition program. The target was

pre-sputtered for 2 min to remove any contamination on its surface and bias striking had been

done for the 30s to check if the plasma was generating properly. Argon pressure of 10 mTorr was

chosen to deposit the gold target at room temperature (25^oC or 298K). 200 W DC power had

been supplied to the system with a ramp time 60s. The argon flow rate was measured to be 25

sccm. The rotation of the substrate about the vertical axis was maintained at 25rpm. In the above-

mentioned condition, the gold target was coated for 200s to complete the sputtering process.
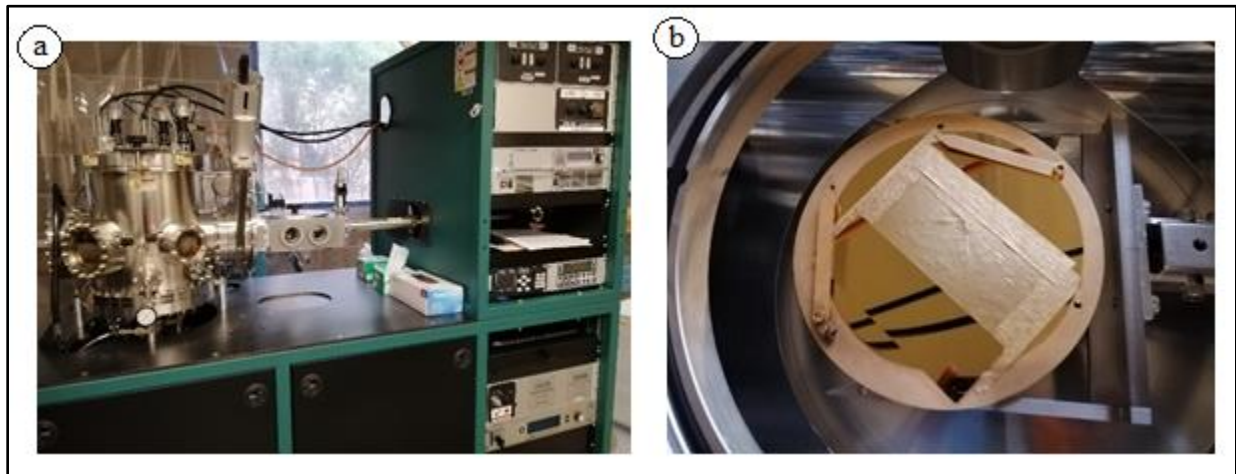
Figure 19: a) AJA ATC Orion 5 Sputtering System, b) After completion of Gold sputtering
inside the sputtering chamber.

3. **Mask removal.** After completion of the sputtering process, the mask was removed

carefully without damaging the sputtered electrodes. Then the wafer along with the electrodes

cleaned carefully with Acetone and dry air to remove any unwanted particles from the top of the

surface of the electrodes. After cleaning the electrodes are ready to use for the experiment. But it should be handled carefully during experiments especially in making electrical connections. The coating is very fragile and tends to wear out easily when comes to contact with hands and copper tape.
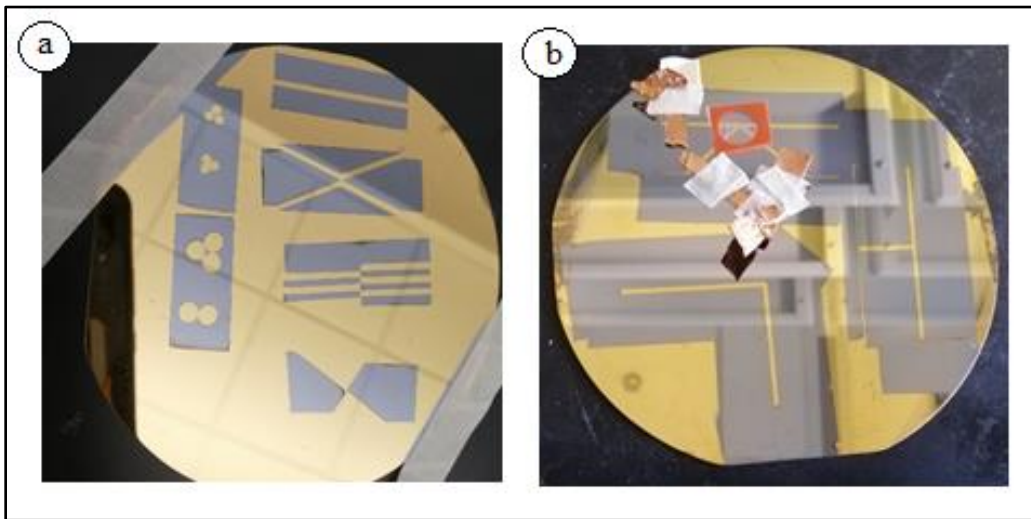
Figure 20: Sputtered electrodes on top of wafer after mask removal.

CHAPTER IV

EXPERIMENTAL PROCEDURE

Experimental set-up

The experiments were carried out at room temperature. First, the fabricated micro-

channel was combined with the micro-electrodes integrated wafer. The soft lithography

fabricated microchannel was combined with silicon wafer by means of adhesion force between

the PDMS and the silicon wafer. The adhesion force is enough for a leakage proof connection.

PTFE tubing was used to supply liquid to the microchannel.

1) Data collection computer,
2) embedded Camera,
3) Optical microscope,
4) Laser source,
5) Syringe pump (liquid supply),
6) PDMS micro-channel/ 3D printed micro-channel,
7) Silicon wafer with Sputtered micro-electrodes,
8) Function generator (AC/DC signal), and
9) Liquid collection tube.
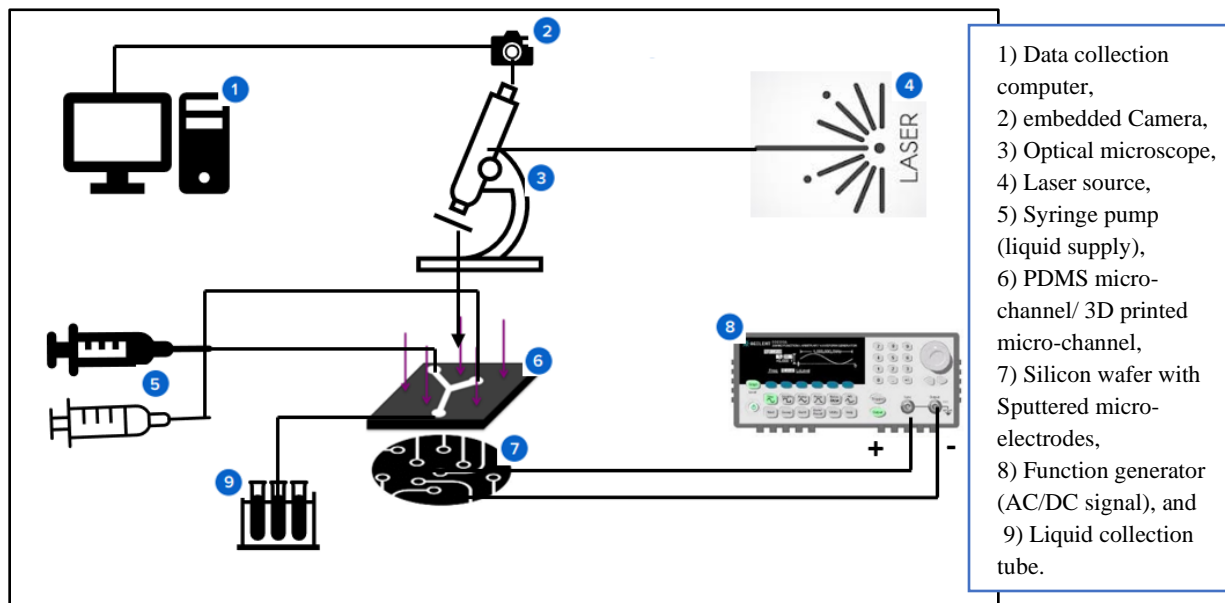
Figure 21: Schematic of the experimental set-up.

Finally, the connector clip from the function generator was connected to the wafer to supply electric current to the microelectrodes in the wafer. The silicon wafer along with the microchannel was attached on top of the microscopic stage (a part Micro-PIV system) using adhesive tape. It was attached under the microscopic lens such a way that the microchannel can be focused to observe fluid movement inside the microchannel. It is illustrated in figure 22. The 3D printed microchannel was combined with a PDMS layer on top as it is transparent to observe the fluid flow movement inside the microchannel. The copper tape was used to create electrodes inside the microchannel. The copper electrodes were sandwiched between the 3D printed part and the PDMS layer. The extended part of the copper tape was used to connect with the connector clip from the function generator. In another arrangement, sharp tip electrodes were used to make the electric connection. It is highlighted in figure 23.
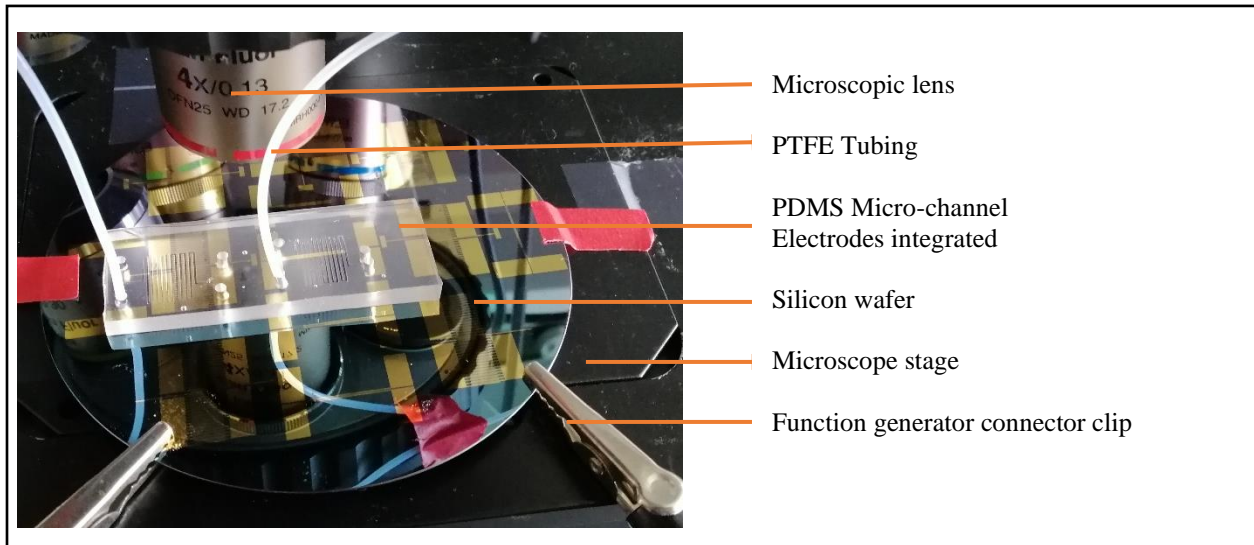
Figure 22: Arrangement of electrodes and microfluidic tubing with the soft-lithography fabricated micromixer.

The schematic of the complete experimental set-up is illustrated in figure 21. The experimental fluid is provided in the microfluidic mixer using a syringe pump through the PTFE tubing. The flow rate and amount of fluid discharged from the syringe pump can be controlled and adjusted based on the experimental requirement. The fluid movement inside the micromixer is observed using the integrated micro-PIV system. This Micro-PIV system consists of a personal computer, an optical microscope with an integrated camera, and a laser unit. The image captured using the camera was stored in the computer and those imaged was analyzed using Insight 4G software to get the velocity vector inside the micromixer. The function generator is used to supply an electric signal in the micro-electrodes.

3D printed part and Separate PDMS layer

Integration of 3D printed part and PDMS Layer

Sharp tip electrodes and PTFE tube connection with the 3D printed microfluidic mixer

Creating electrode connection using copper tape
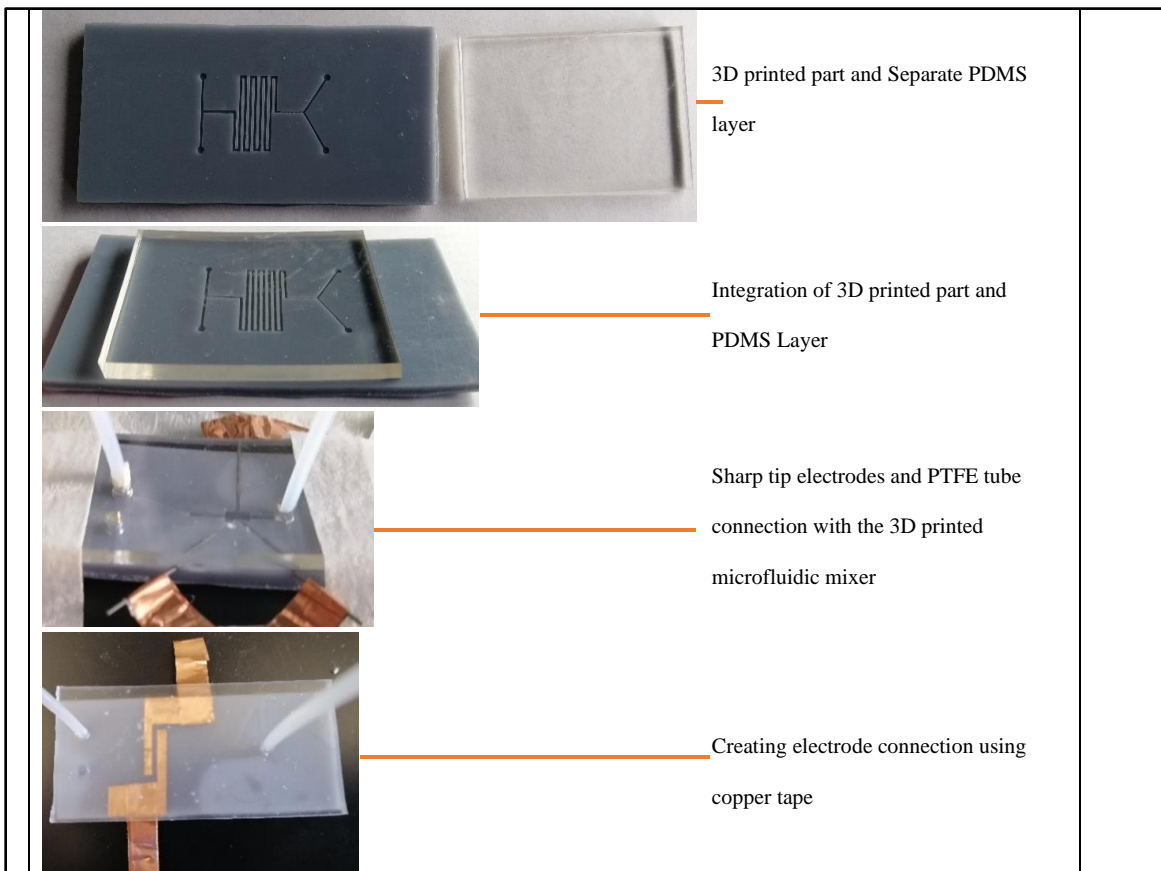
Figure 23:Arrangement of electrodes and microfluidic tubing with the 3D printed micromixer.

Experimental fluid preparation

The experiment was done on dynamic fluid flow through system. Three types of fluid were used in this experiment, i) DI water (10 µS/cm), ii) PBS (Phosphate buffered saline) solution (12 mS/cm) and iii) NaCl solution (50 mS/cm). Low to high conductive solutions were used to test the functionality of the experimental setup within a different range of conductivity. FluoSpheres polystyrene 1.0 µm particles were used as the tracer particle. Before injecting the fluid into the mixing chamber, 1µl of polystyrene particles were mixed with 10 ml of the liquid. These polystyrene particles are excited at a wavelength range from 540-640 nm by exposing under laser light. Then, the particles emit light at a wavelength range of 580-700 nm. which will be captured by an integrated camera in the microscope through an optical filter (XF2017-660DRLP).

Figure 24, shows the plot of capacitance at a different frequency for the three different experimental fluids. Impedance spectroscopy is an essential tool which depends on the electrode pattern and surface roughness. It helps to find out the suitable frequency regions of different ACEK mechanisms (ACEO, ACET & DEP) for different setups and configurations. In this plot, all three fluids with different conductivity showed the same trend. So it is assumed that the effect of frequency will be similar within the range from 10 Hz to 10 kHz, where capacitive impedance dominates and thus ACEO flow will also dominate in this region. Although in the range of 1KHz to 10KHz, capacitance is below 10pF, which means there is a possibility of occurring ACET flow at the same time. Above 10KHz the capacitance is very low, so the effect of ACEO will be diminished and the effect of ACET will start dominating the flows. Above 1MHz, the drastic reduction in capacitance creates a suitable environment for the activation of the DEP effect which can help to trap bioparticles dissolved in the fluid.
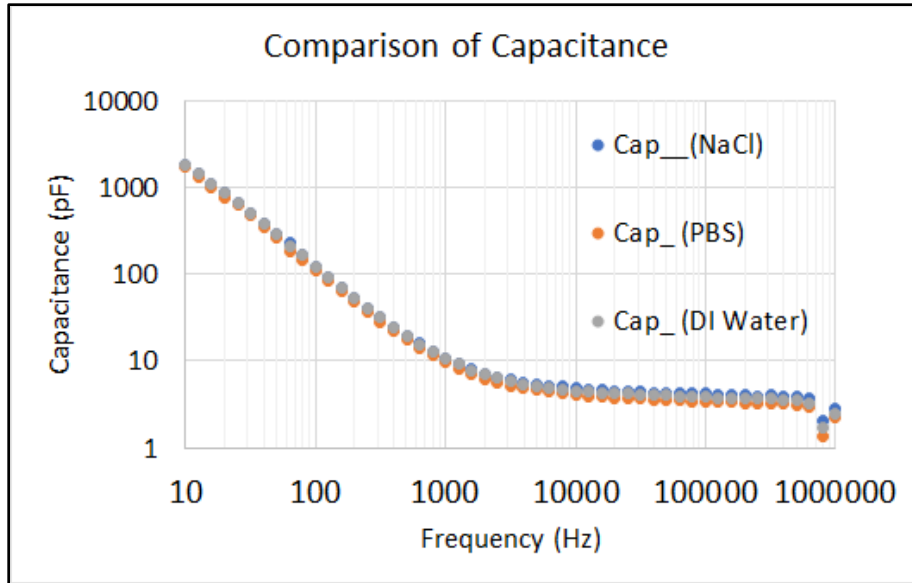
Figure 24: Impedance spectroscopy of different types of experimental fluids.

Flow characterization using the micro-PIV system

To measure the velocity profile across a plane in a microfluidic device, the micro-PIV system is used. It is known as micron resolution particle image velocimetry (Micro-PIV). It uses a volume illumination technique where the laser source and the observation field are introduced through the same channel. The focal plane is moved down through the entire observation area to map the flow field. It is an entire-field, non-intrusive measurement technique where the fluid velocity is measured by recording the displacement of tracer particles (FluoSpheres polystyrene, 1.0 µm diameter) added to the fluid. Thus, it creates a velocity vector field for the desired observation field.

The technique is based on a simple principle. Let us assume a single particle in a fluid flow. The particle is considered to have the same density as the surrounding fluid. The size of the particle is small enough that it follows the flow properly and it does not disturb the flow field. Let us record

the position of a particle at two different time instances which are separated by an interval dt.

The distance covered by the particle in this time interval is expressed by ds. It is assumed that ds

and dt are sufficiently small that the velocity during this small time remains unchanged. The

acceleration occurs during this time interval is ignored. The above situation is illustrated in

figure 24. Then the local fluid velocity can be calculated as below.

$$u \approx \frac{X_{t+\Delta t} - X_t}{\Delta t} = \frac{\Delta s}{\Delta t} \qquad \text{(Eq 20)}$$

This idea can be extended to the whole flow field. In micro-PIV, the experimental fluid is seeded

with small tracer particles. The desired flow field is illuminated by a powerful laser source (light

wavelength, 532 nm). The tracer (fluorescent microbeads) particles are excited by the incident

laser light. These particles emit light of 620nm wavelength. This emitted light is captured by a

CCD camera at two different time instances separated by dt. The single image contains

thousands of these particles. To calculate the position of every particle the entire image is

subdivided into many smaller regions. Each region is analyzed by correlation method to find the

local displacement vector ds. Thus, the velocity vector for the entire field is calculated.
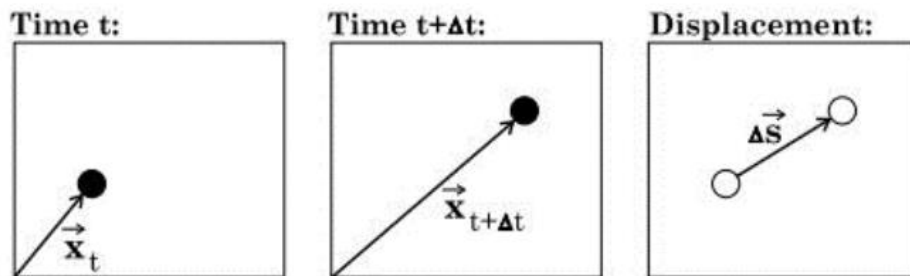
Figure 25: The position of the micro particle at different time instances.

Data acquisition using INSIGHT 4G software
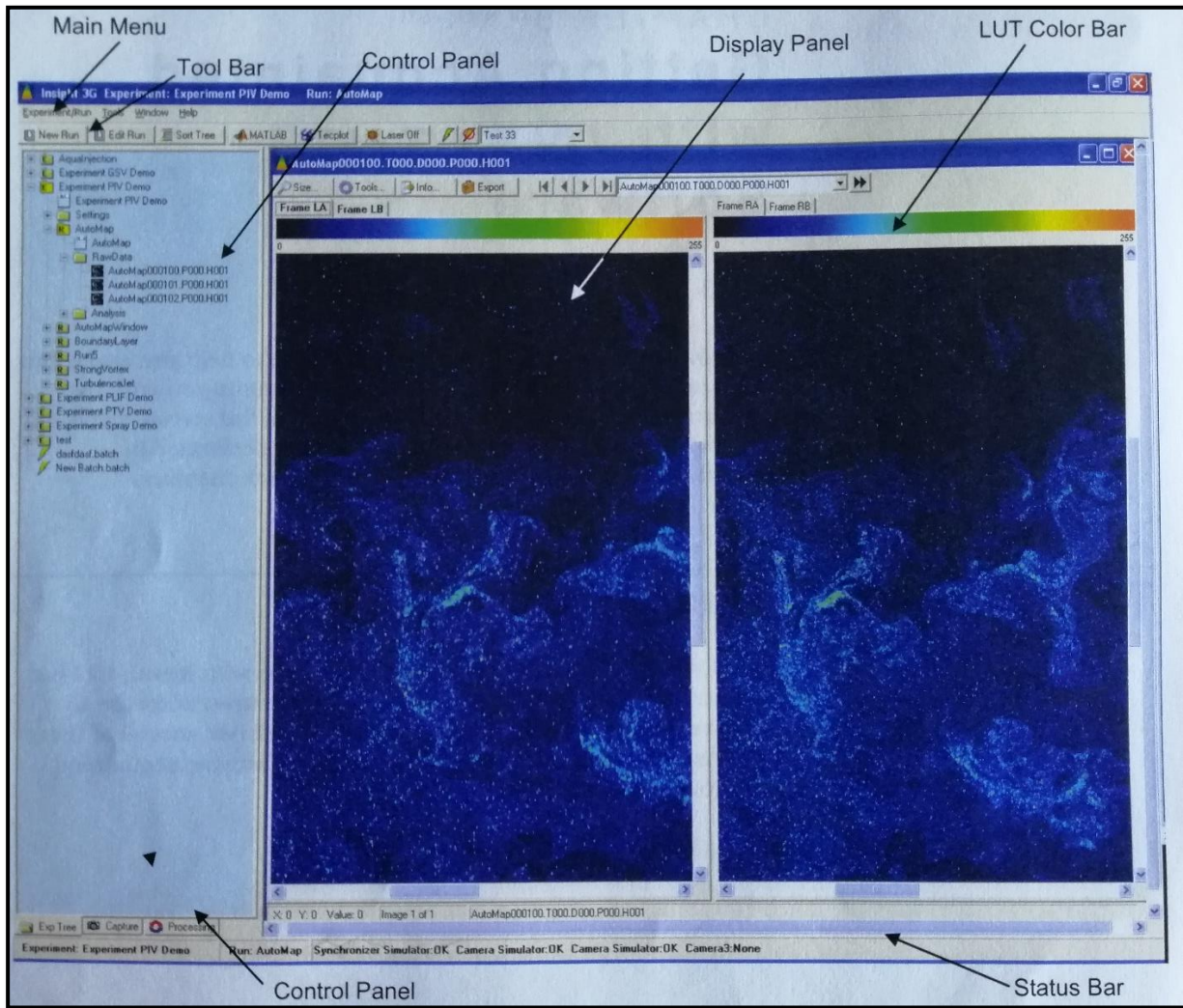
Figure 26: The screenshot of the main window of the INSIGHT 4G software.

INSIGHT 4G software is used for data acquisition. It is a Microsoft windows-based software that is used for global image capture, analysis, and display purposes. It automates the process of image capture, analysis, and data validation for each image. It is used for PIV measurements, PLIF measurements, and global spray diagnostics. It is functionally divided into two parts- an acquisition and processing part and a presentation part. The first acquires an image and processes it to obtain various properties such as velocity vectors, temperatures, or

36

concentration information. The second part displays these results which can be enhanced for optimal viewing. Additional tools such as Tecplot is used for viewing additional information of the flow field. It is used for measuring microflows and making time resolved measurements of flow fields. It can capture simultaneous velocity and scalar property measurements using the same type of cameras to capture particle image and global fluorescence fields. The important steps of data processing are calibration, mask creating, preprocessing, and post-processing. The screenshot of the main window is illustrated in figure 26.

CHAPTER V

EXPERIMENTAL RESULTS

Fabricated Micromixer using soft lithography

After several attempts, the micromixer was fabricated successfully using in house soft

lithography technique. The lowest channel width achieved so far was 300 microns. It is

illustrated in figure 27. It was not possible to go beyond that dimension for the following

reasons. First, the limitation in the mask printing process. A normal office printer is used to print

the mask, which limits the minimum dimension of the channel width. Because in the lower

dimension the quality of the printing resolution decreases rapidly.
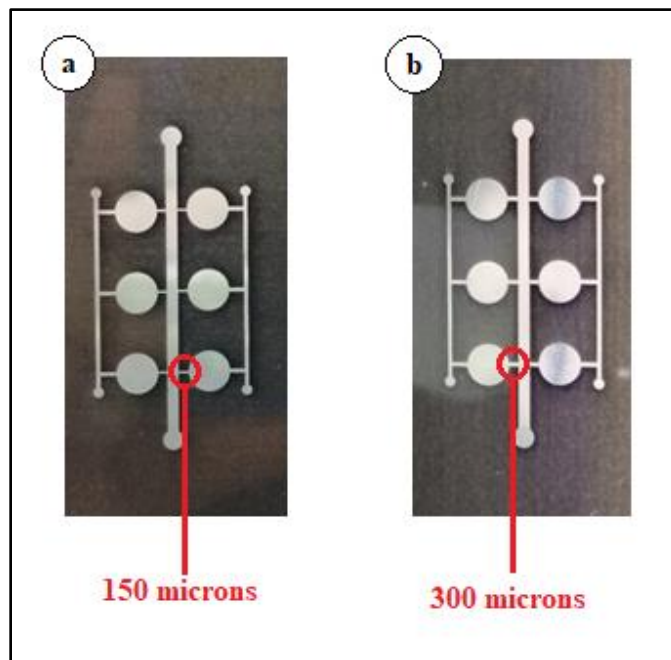
Figure 27: Lowest dimension for mask fabrication.

When the mask in figure 27(a) was used, after fabrication the lowest dimensional was not visible while using the mask in figure 27(b), it was visible after fabrication. Second, another important parameter was the contact aligner. As there was no contact aligner present in our lab. So, the UV exposing was done without using a contact aligner. There was always a gap between the mask and the silicon wafer. This limits the lowest dimension of the microstructure. Third, the UV light used for the experiment was a commercial light that diverse the light. That creates two light circles emitted from the UV light. The inner circle has the highest intensity light. The inner circle is smaller which restricts the amount of area exposed by the UV light.
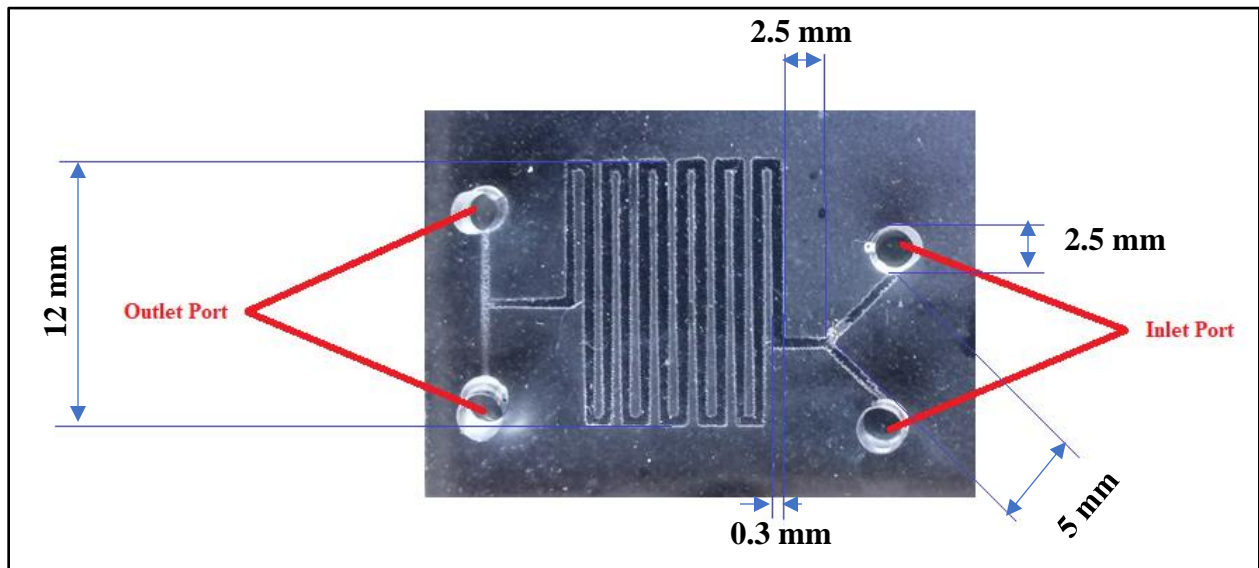
Figure 28: Soft lithography fabricated passive micromixer.

Finally, the soft lithography fabricated micromixer is illustrated in figure 28. The depth of the channel was 40 microns. It was the lowest achievable channel depth using photoresist SU-8 2025. The nominal channel thickness was 300 microns. It is a passive micromixer. It has two inlets to support two different fluid input. It has a total of 135 mm mixing length to support the mixing properly. It uses the geometrical advantages to do the mixing.

Microscopic analysis of the micromixer

A microscopic view of the micromixer shows that it has some irregularities at edge of the channel. It will create obstacles in the fluid flow. So, the target is to make the edges as smooth as possible. These edges were created due to low resolution mask. It is shown in figure 29, that the plastic mask has a similar edge to final PDMS micromixer. The UV light passed through the irregular edges of the mask. To reduce those irregularities high resolution printer is recommended to use for mask printing.
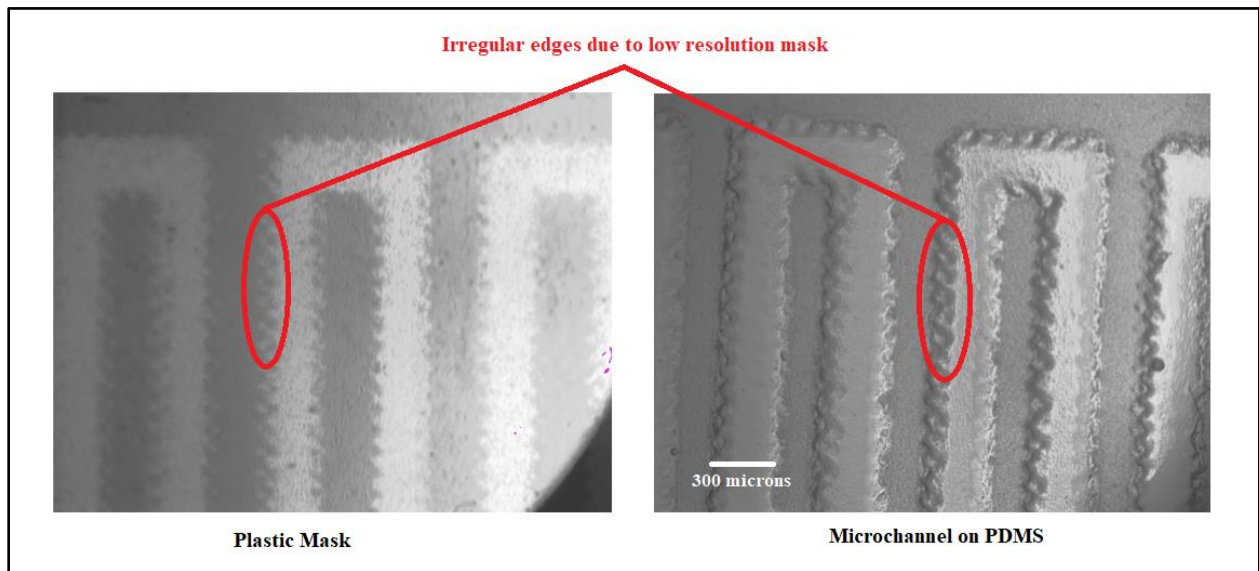
Figure 29: Microscopic view of the microchannel edges

It was also observed that some portion of the micromixer has some irregularities like the microchannel in some areas was not properly developed. It is due to the intensity difference during UV exposure. The UV light used in this experiment has two different light intensity zone. During UV exposing it might occur that some part of the micromixer was not get proper UV

light. For this reason, some portion of the micromixer like inlet, T-section and some edges were not properly developed. It was illustrated in figure 30.
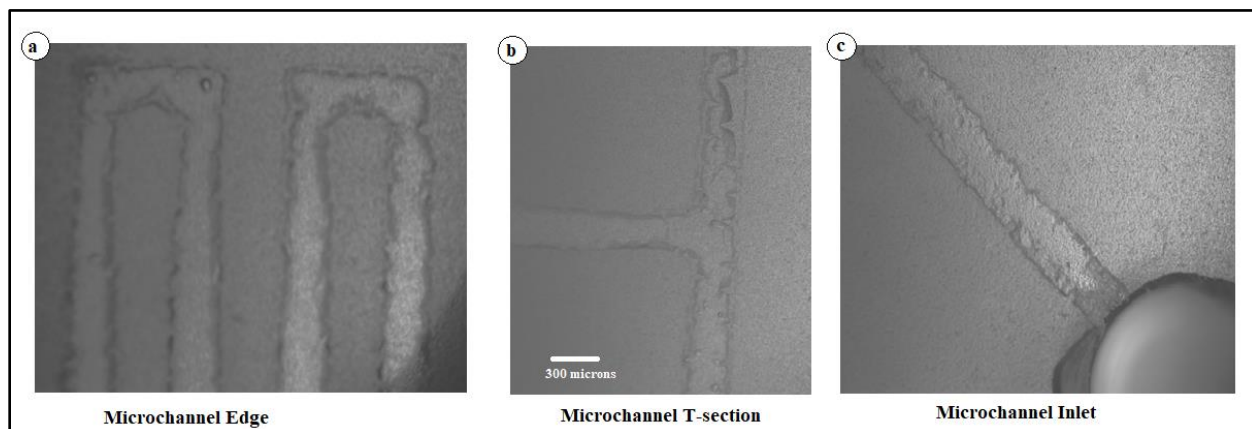
Figure 30: Irregularities in micromixer fabrication.

Fabricated Micromixer using 3D printing

Both active and passive micromixer was fabricated using a 3D printer. It is illustrated in figure 31. The active micromixer (figure 31 (a)) has the four minor channels connected to the mixing chamber. The purpose of these minor channels is to create space for sharp electrode insertion. The sharp electrodes were inserted through these minor channels to create electrokinetic in the mixing chamber. The passive micromixer has a similar design that has been used in soft lithography fabrication. The channel depth of these micromixers is 500 microns. This is very large compared to soft lithography fabricated micromixers. Although the 3D printer used in this experiment can lower than this dimension. But for the present experimental condition, 500 microns is used as the lowest dimension for 3D printing. In the future, I have planned to go lower dimensions to fabricate a microfluidic mixer.
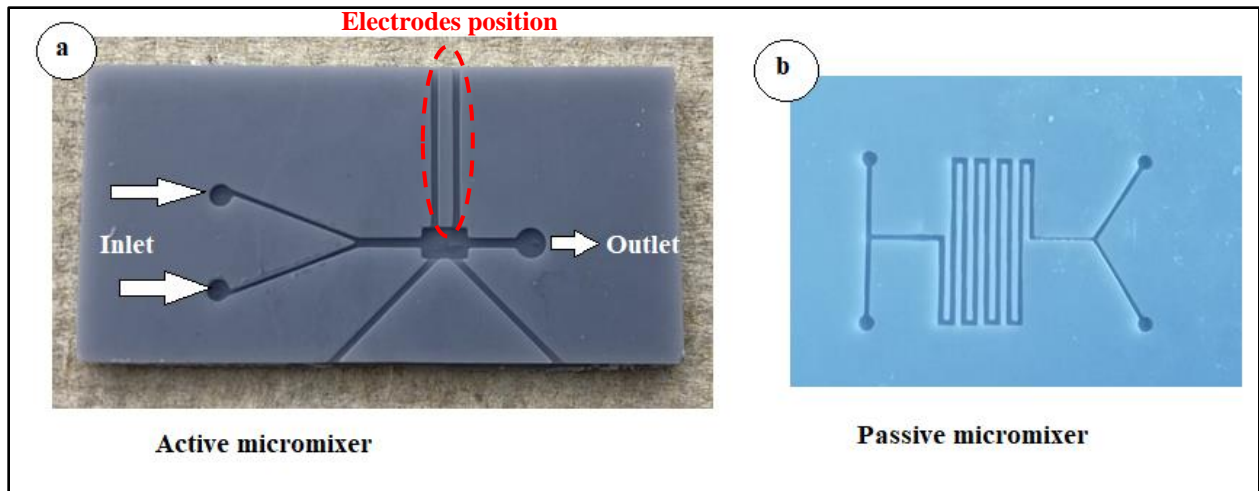
Figure 31: 3D printed micromixer

Microscopic view of the 3D printed micromixer

The microscopic view is important to analysis the internals of the micromixer. Flow-through a microfluidic chamber is largely dependent on the surface and the smoothness of the channel. Because viscus force is dominant in the microfluidic mixer which governs fluid flow patterns. And the mixing in the microscale strongly depends on the fluid flow pattern. The fluid flow pattern depends on the surface of the microstructure. The microstructure of an active micromixer is illustrated in figure 32.
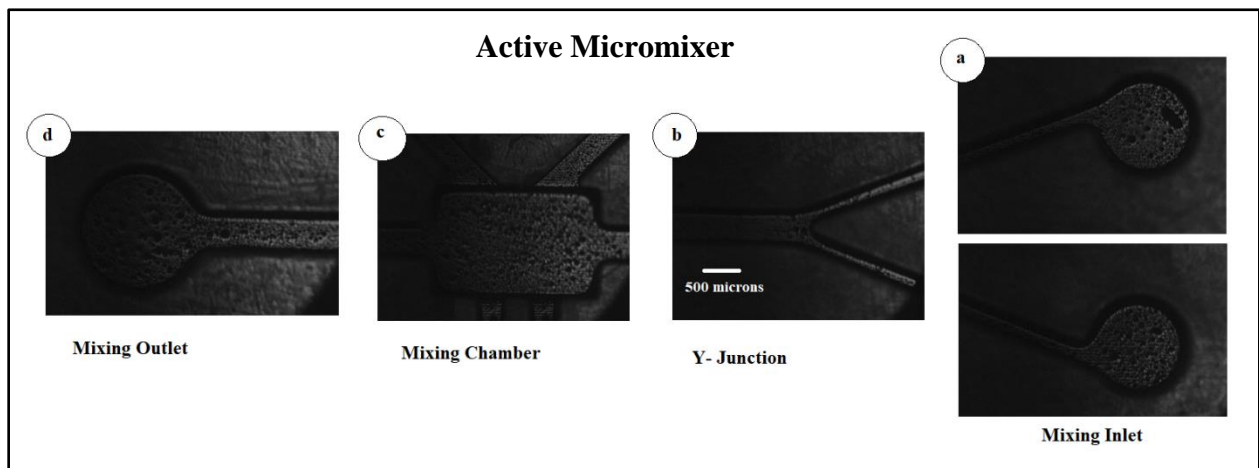
Figure 32: Microscopic view of the 3D printed active micromixer.

It was observed that the internal surface of the micromixer is not smooth. There are small porous points observed on the internal surface. These porous points attract the water molecules due to adhesion force. These create hindrance in the fluid flow which is also responsible for low mixing between two different streams of fluid. The smoother the surface of the internals, the better it creates a favorable environment for microfluidic mixing. The surface of the 3D printed microfluidic device depends mostly on the photopolymer resin used during 3D printing. This resin is specially designed for reducing volume shrinkage during the photocuring process, which ensures the high precision of the print model with a smooth finish. If the surface roughness of the microstructure is needed to be improved, a better-quality resin is needed to be used. The microscopic view of the 3D printed passive micromixer is presented in figure 33.
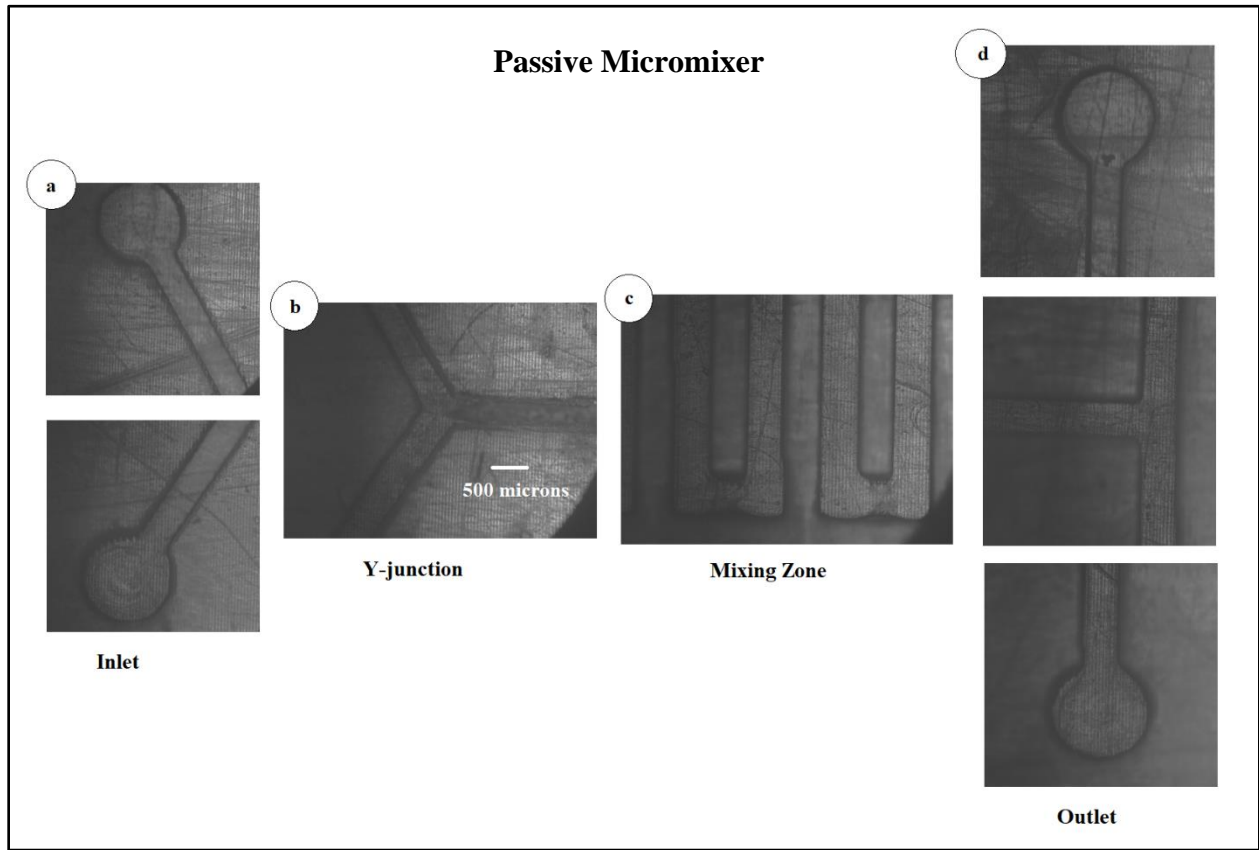
Figure 33: Microscopic view of the 3D printed passive micromixer.

Fluid flow through the micromixer and leak test

After completion of fabrication, the micromixer needs to be tested for flow through

system and possible leak test in the channel. Potassium permanganate solution was used to make

colored water solution. Then the colored water passed through the micromixer by using a syringe

pump. It is illustrated in figure 34 (b). It is observed that the colored water passed easily through

the micromixer. The is no observable leak found in the micro mixer.
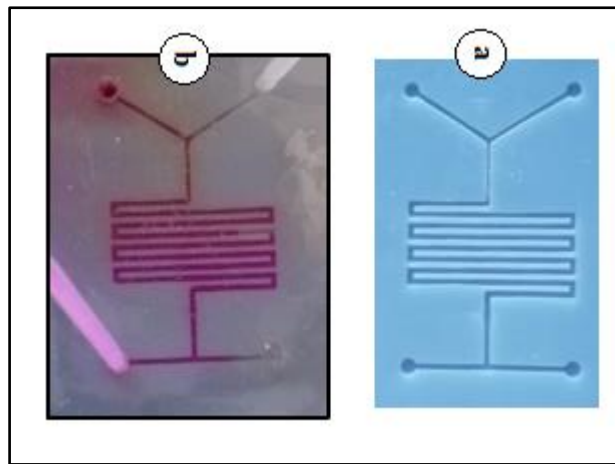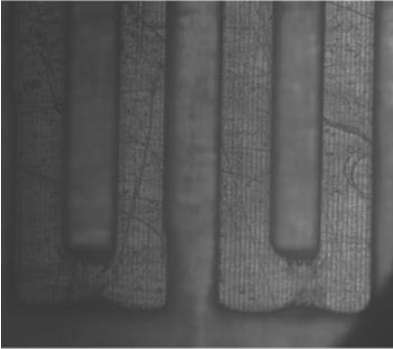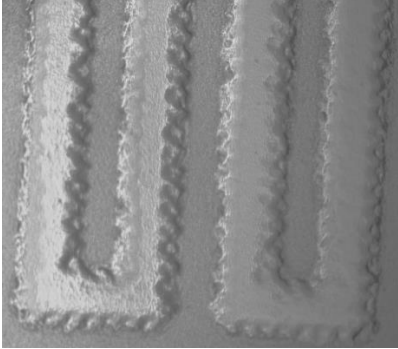
Figure 34: Leak test through the micromixer.

Comparison between 3D printing and soft lithography microfabrication

Two micro fabrication technique was used in this experiment. One is soft lithography and

other one is 3D printing. Both are very popular microfabrication techniques among researchers.

The 3D printing technique is the most recent and advanced method. Apart from that, each

technique has their advantages and disadvantages. In table 1, it is discussed based on the

fabricated device based on those techniques.

Table 1: Comparison between 3D printing and soft lithography microfabrication.

3D Printing Microfabrication	Soft lithography Microfabrication
The wall of the microchannels has a smooth finish and has almost no irregularities	The wall of the microchannels has a rough finish and has many irregularities
The surface of the microchannels is rough	The surface of the microchannel is smooth
Smaller dimensions are very difficult to achieve	Smaller dimensions can be achievable
Fabrication time very short. For this experiment, it took 25 minutes to print	Fabrication time is very long. It took almost 150 minutes to fabricate.
The fabrication process is easy and has three steps	The fabrication process is complex and has 12 steps
The only raw materials used is photopolymer resin	There are more than five raw materials involved
The raw material is cheap. So, the total fabrication cost is low	The raw materials are expensive. So, the fabrication cost is high
The only equipment needed is the 3D printer	There is several equipment needed like spin coater, vacuum pump, UV exposer, developer station, heating arrangement etc.

Integration with microelectrodes is difficult. As the 3D printed materials is not suitable for sputtering	Integration with microelectrodes is easy as the wafer can be easily used for sputtering microelectrodes
The 3D printed material is not transparent. So, another layer of transparent PDMS is needed.	Transparent materials like PDMS can be directly used for microfabrication
The 3D printed material is not a suitable flexible lab on a chip device	It is suitable for flexible lab on a chip device
This technique could be used for complex lab on a chip device	This traditional technique is not suitable for complex lab on a chip device

Surface hydrophobicity test

The velocity of the microscale flow largely depends on the interfacial resistance faced by the liquid from the solid surface. The interfacial resistance depends on the surface wettability. The surface wettability can be measured in terms of contact angle and droplet wetting length. The droplet wetting length increases if the contact angle decreases. The contact angle defines a surface is whether hydrophilic or hydrophobic. It is illustrated in figure 35.
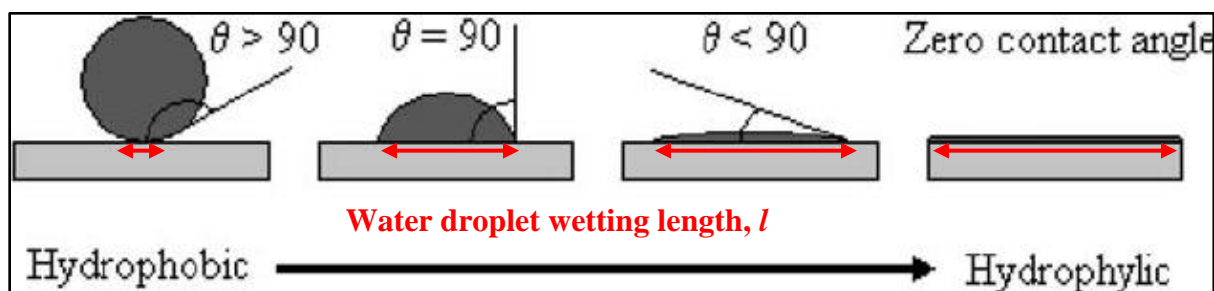
Figure 35: Relation between droplet wetting length and hydrophobicity.

To get an idea about the surface interfacial resistance, a 2.0 µl water droplet is attached to the four different surfaces (PDMS, Glass, Wafer, Photopolymer). After putting the droplet on to the surfaces, the individual microscopic image was captured using a microscope embedded camera. The width of the droplet was measured in terms of pixel length. It defines the water droplet wetting length. It was found that the PDMS surface is more hydrophobic than the photopolymer surface. It means the water will face less resistance during microscale flow on top of the PDMS surface than the photopolymer surface. Because the droplet wetting length is larger (1600 pixels) for the photopolymer surface than the PDMS surface (1300 pixels). It is illustrated in figure 36. So, it can be concluded that the soft lithography fabricated micromixer requires less fluid driving pressure than 3D printed micromixer.
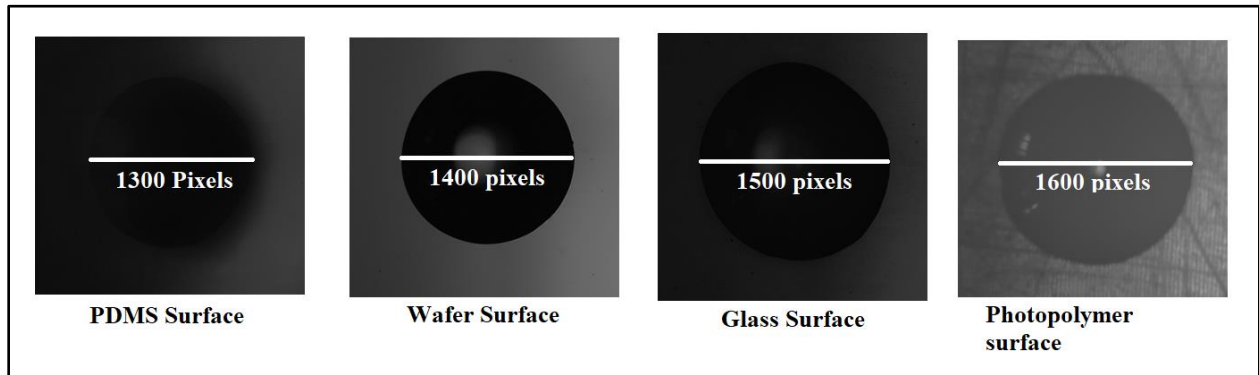
Figure 36: Hydrophobicity test of different surfaces.

Flow characterization using the micro-PIV system

1.   **Active micromixer.** For experimental analysis, the average inlet velocity was 212 µm/s. The calculated Reynolds number was 0.178. This small Reynolds number created a laminar profile in the channel. In figure 37, it is observed that the fluid flow pattern is completely laminar. In this condition, the fluorescent particles in the fluid does not have the ability to go to the adjacent layer of the fluid.
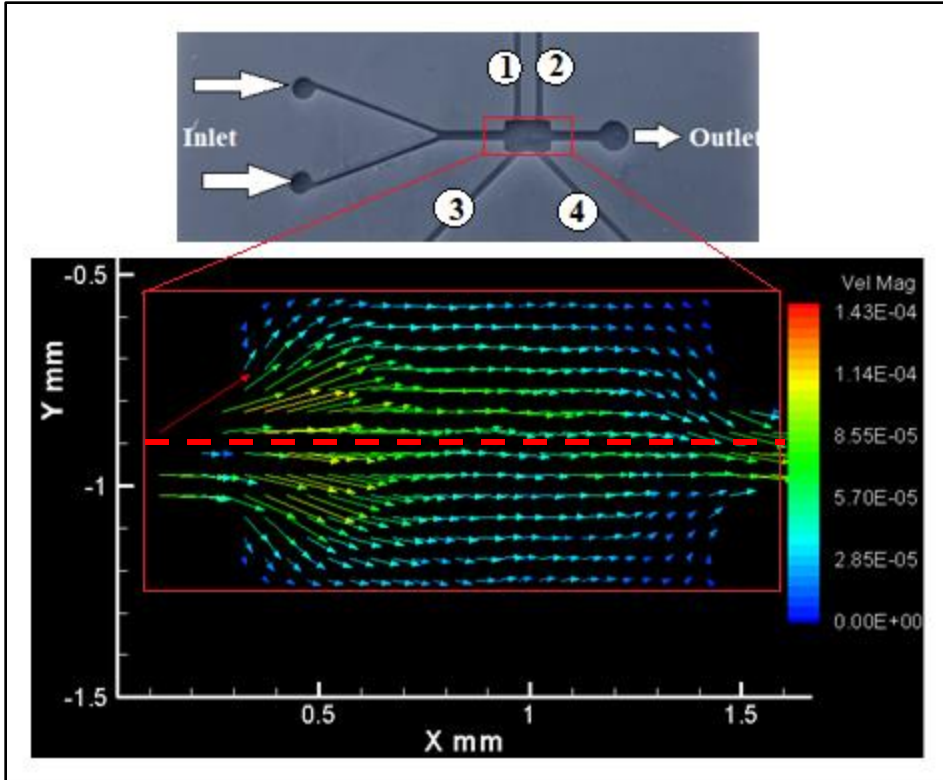
Figure 37: Fluid flow direction inside micromixer without electric field

An imagined red line was drawn in the middle of the channel to differentiate between the two fluid streams. It is observed that after going out from the mixer zone of the micromixer the upper part of the fluid stream remains in the upper part of the microchannel and the lower fluid stream remains in the lower part. After that the AC electric field was applied to the electrodes. It was started from 2 V p-p and continued until 5 V p-p. It was found that there was no notable deflection was found in the flow pattern until 2 V. In figure 38(a), it is observed that the flow field is changing directions at 2 V_{P-P}. Near electrode #1, the electric field force the velocity streamlines towards the middle of the channel. It forces the fluorescent particles in the fluid to go to the adjacent layer and mix with that layer. Similar flow disturbance was also observed near the electrode #2 and #4. These flow disturbances were responsible for changing the velocity vector

48

patterns in the mixing zone. Some flow reversal was observed in that region. It created a mixing environment for the nearby particles in the fluid. So, the direction change in the velocity profile means that the particles in the fluid are mixing with the adjacent layer of the fluid. It is not possible without applying electric potential in the fluid. The effect of frequency in the mixing was also observed experimentally. AC electroosmosis is more dominant in the low frequency range. Because the impedance between two electrodes is capacitive when the applied frequency is low. It becomes resistive in nature when applied frequency is increased. In figure 38(b) and 38(c), it is observed that the electric voltages increase from 3 V to 5 V and the frequency is increased from 100 Hz to 1000 Hz, the disturbances created by the electric field on the fluorescence particles found different from one another. The AC electric field created a wave like flow pattern inside the micromixer. This is wave like flow is responsible for mixing to have occurred at the outlet of the micromixer. The upper fluid stream goes to the lower part of the micromixer and again comes back to the upper part of the microchannel. It creates a sine wave flow pattern in the mixing zone. This sine wave flow pattern becomes more intensified in figure 38(c). So, increasing the voltage and frequency intensified the mixing process in the micromixer. The sine wave flow pattern is highlighted by a white dotted line in figure 38(b) and 38(c).

2.   **3D printed passive micromixer.** Flow dynamics inside the micromixer is illustrated in figure 39 and 40. When two fluid streams meet each other at the Y-junction of the mixer, they tend to flow parallel to each other. They do not mix with each other as the direction of the flow does not change. If we imagine a boundary line in the middle of the channel which separates two fluid streams from each other. It is represented by a red dotted line in figure 39. It is observed that in the straight part of the channel the velocity vector does not change direction.
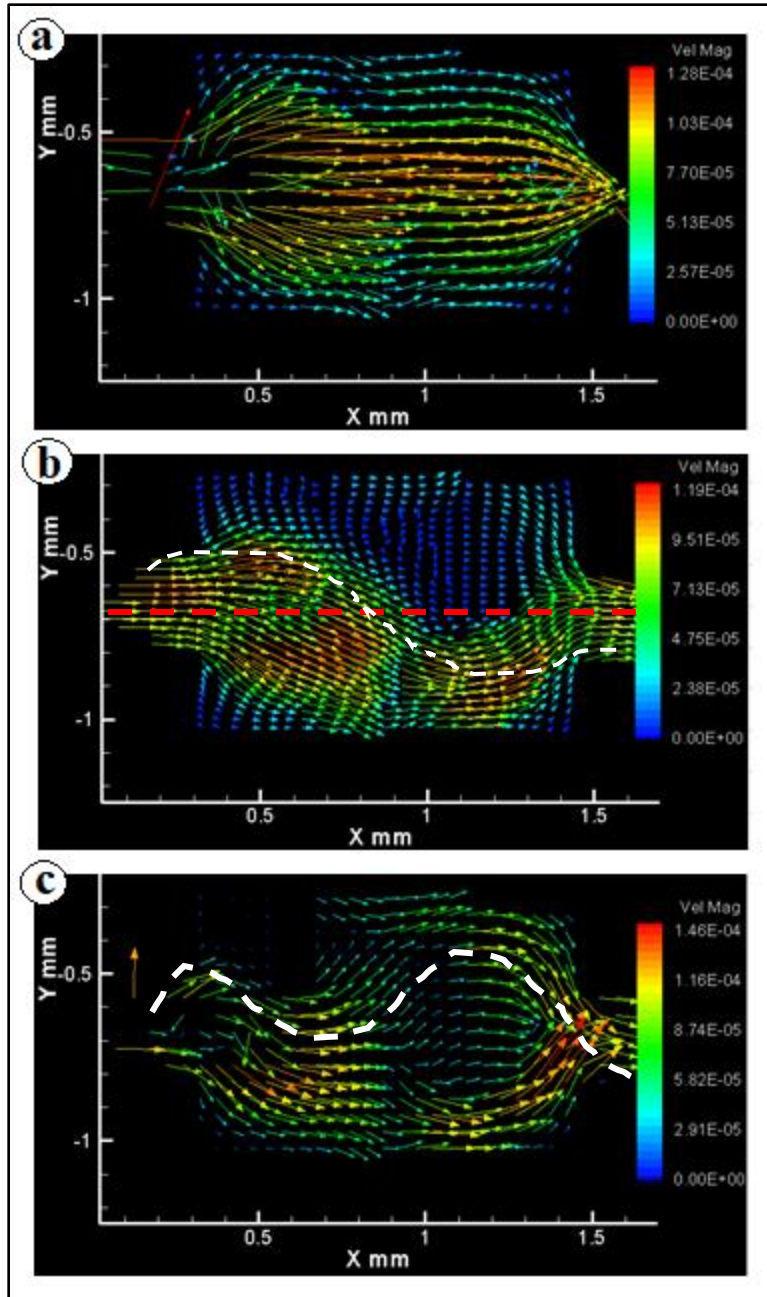
Figure 38: a) flow field inside the channel at ac-potential, v= 2 v & frequency, f= 100 Hz. b) flow field inside the channel at ac-potential, v= 3v & frequency, f=500 Hz. c) flow field inside the channel at ac-potential, v= 5v & frequency, f=1000 Hz.

It means the upper fluid stream remains in the upper portion of the channel and the lower fluid stream remains in the lower side.
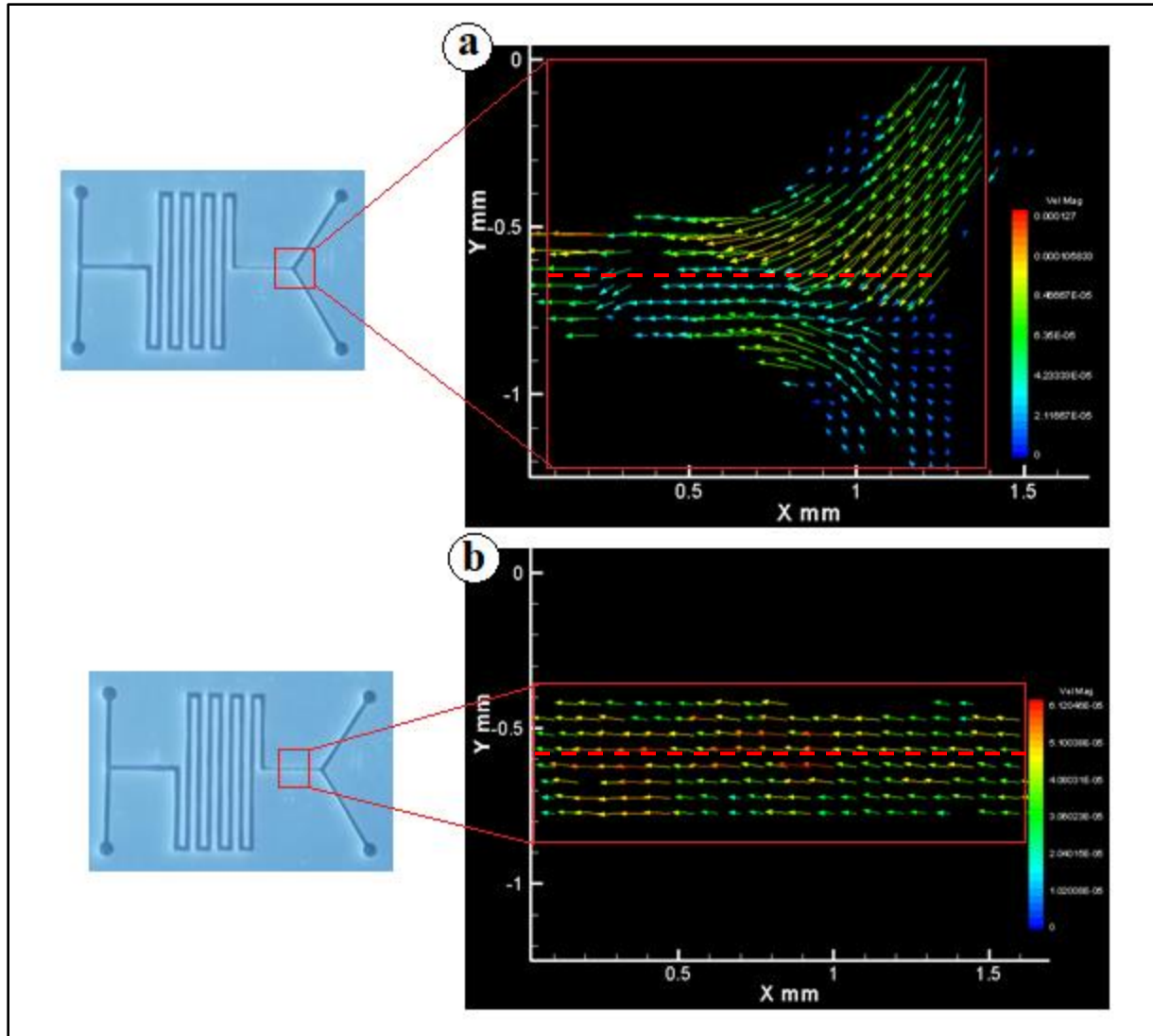
Figure 39: Fluid velocity vector inside the 3D printed micromixer. (Part 1)

The lower fluid stream moves to the upper portion of the microchannel after passing bend 1. It is

highlighted by the red dotted line in figure 40(a). The same event also occurs in bend 2 (figure

40(b)). The fluid velocity vectors change the direction more vigorously in bend 3. The upper

fluid stream goes to the lower part of the microchannel and comes back to the upper portion

again. This increases the contact between the two-fluid stream. As a result, the two fluid streams

mix with each other. This is also true for the subsequent bend of the micromixer. So, ultimately a

mixer of fluid is observed at the outlet of the micromixer.
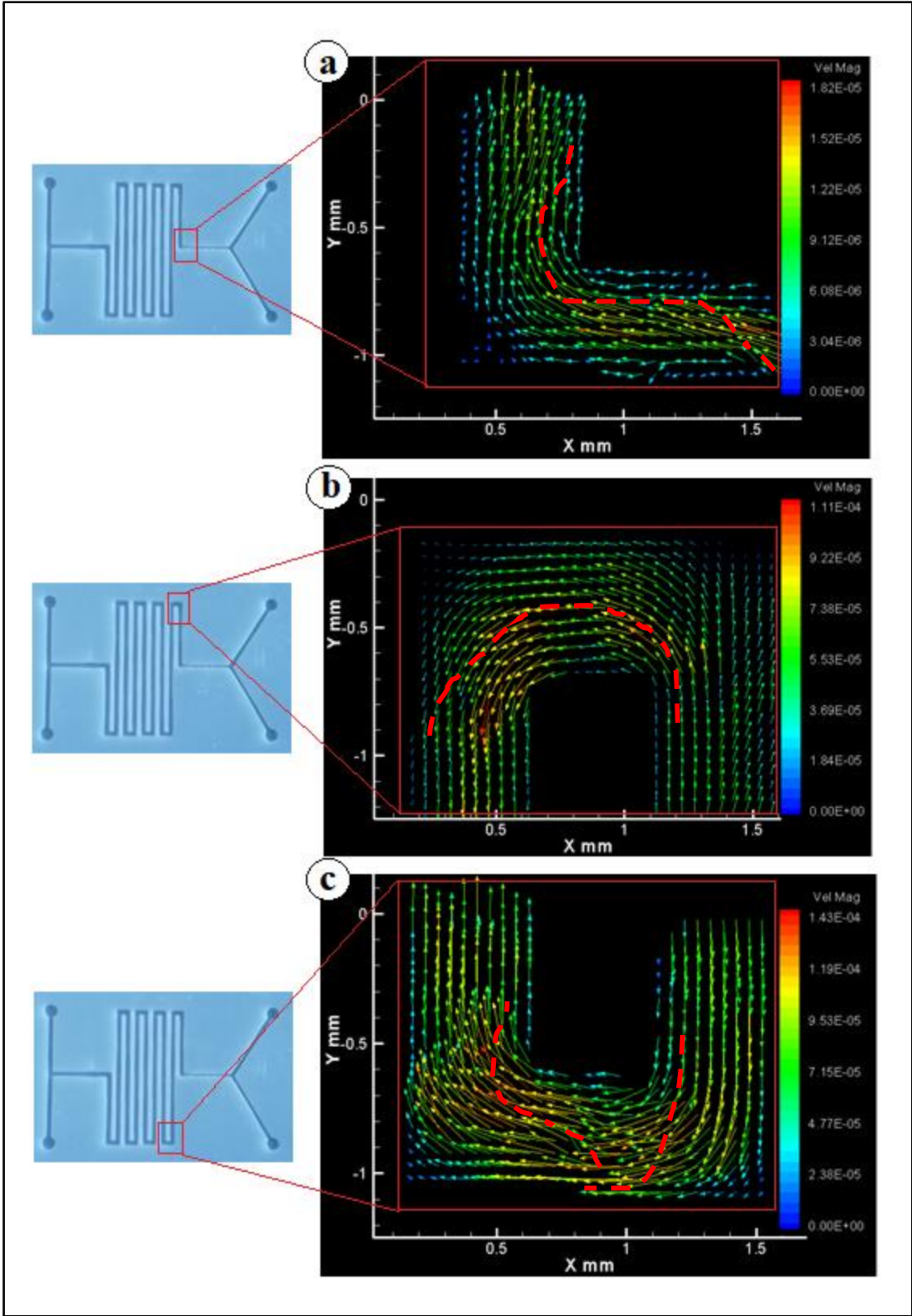
Figure 40: Fluid velocity vector inside the 3D printed micromixer. (Part 2)

CHAPTER VI

NUMERICAL SIMULATION

Microfluidic flows occur on length scales that are orders of magnitude smaller than macroscopic flows. Manipulation of fluids at the microscale has several advantages – typically microfluidic systems are smaller, operate faster, and require less fluid than their macroscopic equivalents. In general, as the length scale of the fluid flow is reduced, properties that scale with the surface area of the system become comparatively more important than those that scale with the volume of the flow.This is apparent in the fluid flow itself as the viscous forces, which are generated by shear over the iso-velocity surfaces, dominate over the inertial forces. The Reynolds number (Re) that characterizes the ratio of these two forces is typically low, so the flow is usually laminar. In many cases, the creeping (Stokes) flow regime applies (Re«1). Laminar and creeping flows make mixing particularly difficult, so mass transport is often diffusion limited, but even in microfluidic systems diffusion is often a slow process. This has implications for chemical transport within microfluidic systems. The Microfluidics Module of the COMSOL simulation software is designed specifically for handling momentum, heat, and mass transport with special considerations for fluid flow at the microscale. COMSOL's general-purpose Multiphysics features are uniquely suited for handling the many microscale effects that are utilized in microfluidic devices. It is easy to set up coupled electrokinetic simulation including electrophoresis, electroosmosis, and electrowetting.

Workflow for modeling microfluidic devices

To model a microfluidic device, it was begun by defining the geometry in the software by importing a CAD file or via the geometry modeling tools that are built into COMSOL Multiphysics. For importing geometry models, several choices can be used: the CAD Import Module, for import of mechanical CAD models; the ECAD Import Module for import of electronic layouts; and the LiveLink™ products for CAD for a direct link to models created in a dedicated CAD software package. In the next step, appropriate fluid properties and a suitable physics interface are chosen. Initial conditions and boundary conditions are set up within the interface. Next, the mesh for the geometry is defined. In many cases, COMSOL's automatically created default mesh, which is produced from physics-dependent defaults, will be appropriate for the problem. A solver is selected, again with defaults appropriate for the relevant physics, and the problem is solved. Finally, the results are visualized after completion of computation. The steps are described in detail below

1. **Geometry definition.** The geometry for both 2D and the 3D mixer was designed. The 2D geometry is designed using the COMSOL built-in drawing tool. A simple straight rectangular channel was designed for numerical computation for the optimization of computational time and resources. It is illustrated in figure 41. AL is used as inlet and FG is used as an outlet boundary. AF is used as the upper wall and LG is used as a lower wall. BC, DE, KJ and IH are the locations of the electric field. Fluid flow direction is assumed as AL to FG. The total length of the micromixer was AF=LG= 100 µm. Dimensions are denoted by alphabets rather than numeric as it was varied for different simulations.
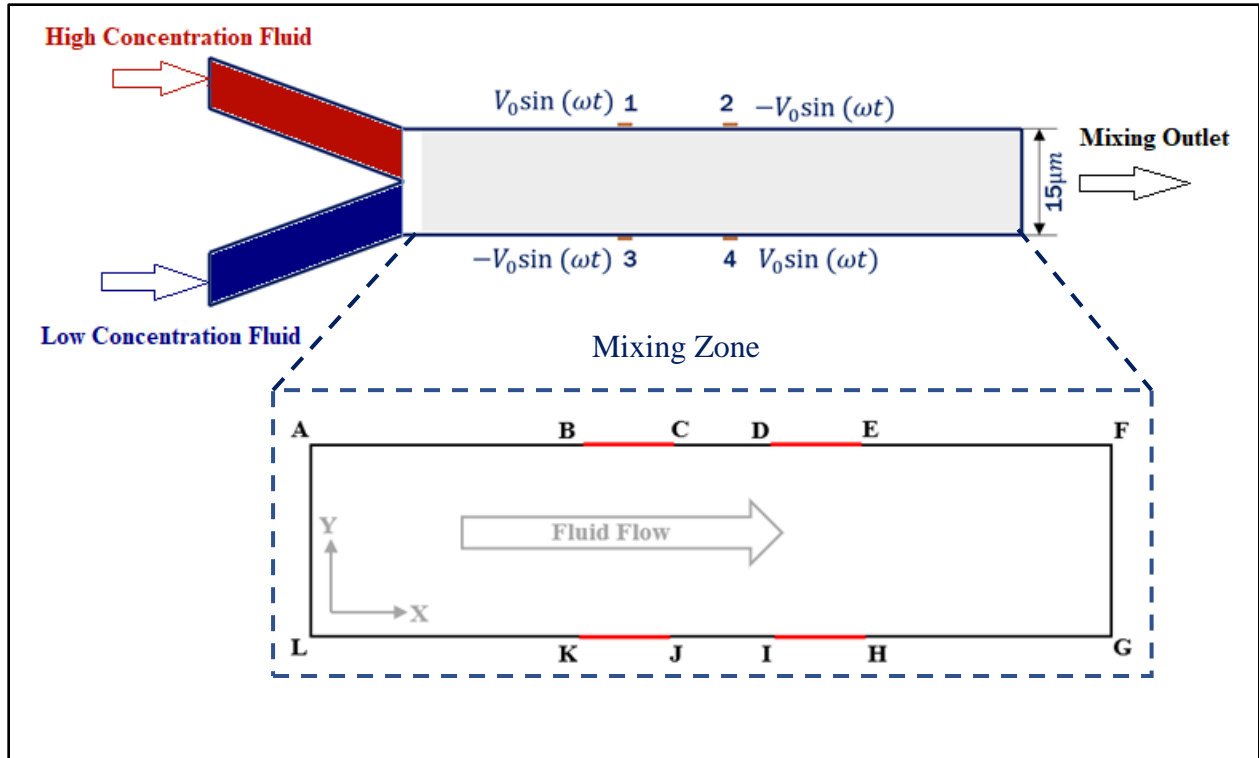
Figure 41: Geometrical model of the 2D micromixer.

Cad tool (AutoCAD 2020) was used to draw the 3D geometry of the micromixer model. Two types of 3D micromixers were drawn using the cad tool. One model is used for passive micro-mixing where no electric field is applied. The mixing is taken place due to the geometrical shape of the micromixer. It is illustrated in figure 42. It has an effective mixing length of total 135.0 mm. It uses the advantages of the advection effect due to 18 right turns in its way from inlet to outlet.

Another micromixer model was designed for active mixing purposes applying the electric field. It is illustrated in figure 43. The length of the effective mixing zone is 27.0 mm. Electrodes are placed in the middle of the mixing zone. Two electrodes are separated by 200 microns from each other. The electrodes were placed like plates in the channel wall to manipulate the fluid in the

channel. So, a total of three different were used in this experiment to observe the mixing in a microfluidic channel.
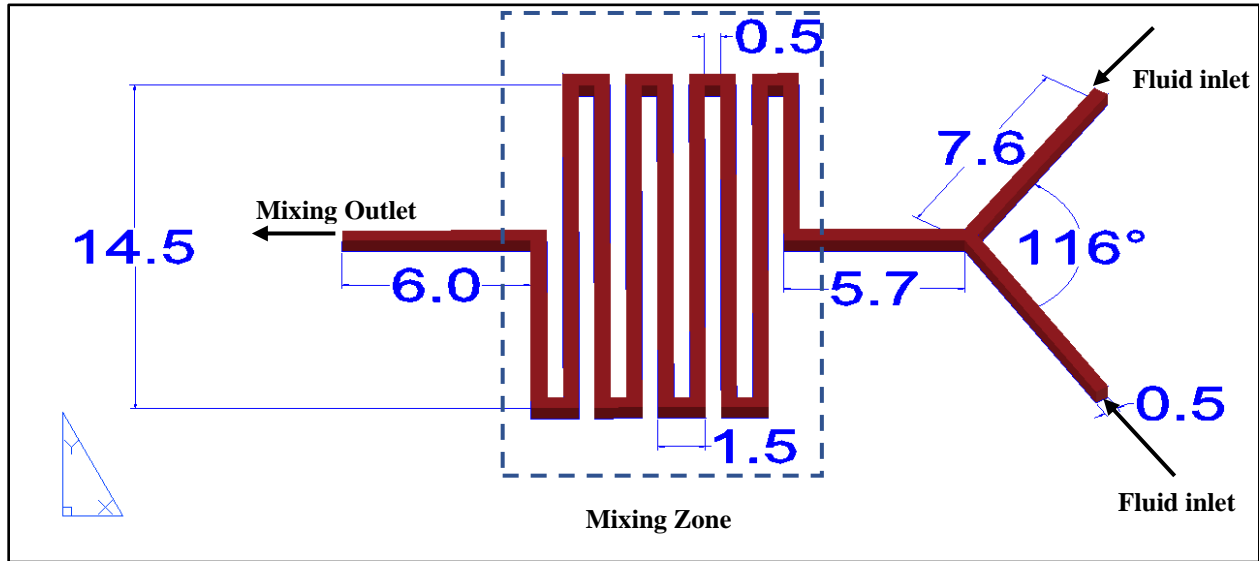
Figure 42: Geometrical model of 3D passive micromixer.
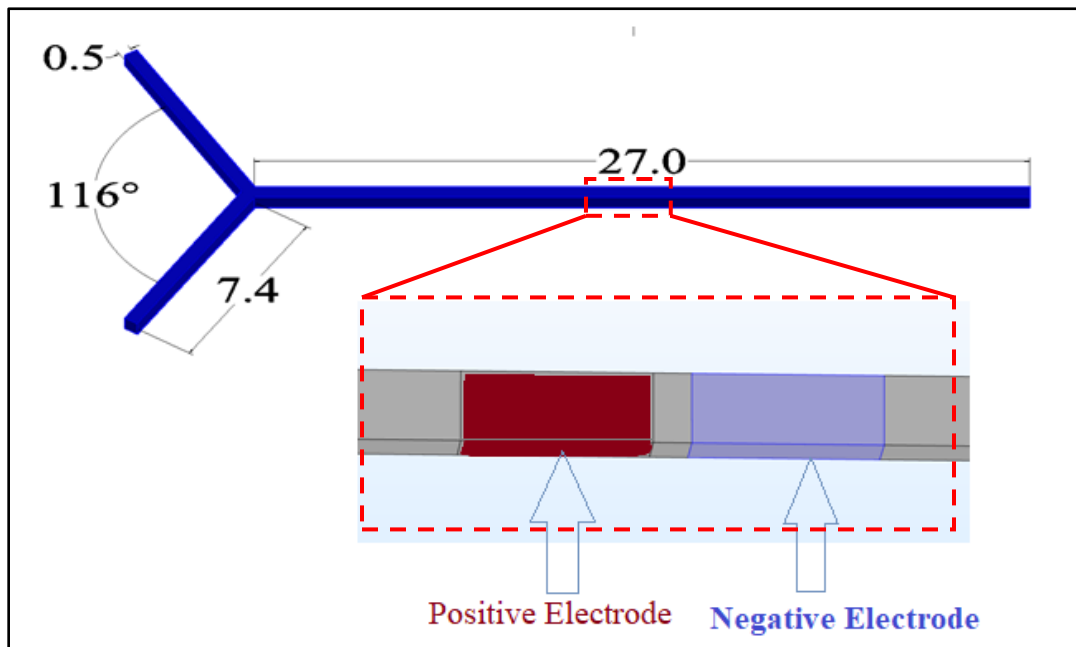
Figure 43: Geometrical model of 3D active micromixer.

2. **Simulation parameters.** In the experiment, water is used as an experimental fluid. So, in the numerical simulation, it is also used as an experimental fluid. But as the electric field and transport phenomena will be coupled with the fluid flow certain fluid parameters must be chosen carefully to run the simulation properly. Two important for the experiment are diffusion coefficient and zeta potential. These parameters are selected based on the previous simulation done by the researchers and published articles. The parameters are presented in table 2. These are used for both 3D and 2D numerical simulations. For the passive micromixer simulation, electric field is not needed. So, the electric field is uncoupled during passive micromixer simulation.

Table 2: Simulation parameters

Name	Value	Unit	Description
U0	0.1	[mm/s]	mean inflow velocity
sigma_w	0.11845	[S/m]	conductivity of the ionic solution
eps_r	80.2		relative permittivity of the fluid
zeta	-0.1	[V]	zeta potential
V0	0.1	[V]	maximum value of the ac potential
omega	2*pi[rad]*10	[Hz]	angular frequency of the ac potential
t	0	[s]	start time
D	1.00E-11	[m^2/s]	diffusion coefficient of the solution
c0	1	[mol/m^3]	initial concentration

3. **Boundary condition**. The fluid is assumed to be Newtonian and incompressible. Flow is laminar and unsteady. The governing equation fulfilling this condition is known as the Naiver-Stokes equation and the continuity equation (Eq 1).

Inlet: At the inlet AL, a fully developed flow condition is applied with an average velocity U0**.**

Wall: Electroosmotic velocity boundary condition is applied at the wall AF and LG using the Helmholtz-Smoluchowski equation. it was derived in the earlier equation (Eq 19). The electric

field is varied with time and applied at the normal to the fluid flow. Electric field is applied in the

wall with a selected position at the magnitude of V0.

Outlet: flow is considered a pressure-driven flow. The pressure is set as $p_0 = 0$ Pa at the outlet

FG.

Electric field: It is assumed that there are no concentration gradients in the ions that carry the

current. So, the balanced equation for current density can be expressed with Ohm's law.

$$\nabla.(-\sigma\nabla V) = 0 \qquad \text{(Eq 21)}$$

Here, σ is expressed as the conductivity of the medium and the term in the parentheses is

represented as current density. Time-dependent electric applied at the electrodes.

At the electrode BC and IH, electric potential V=V$_0$ sin (ωt), at the electrode KJ and DE,

electric potential V= -V$_0$ sin (ωt). ω is defined as the angular frequency of the AC electric

potential. All other boundary is considered as insulated. The insulation boundary condition is

defined by the following equation.

$$-\sigma\nabla V.n = 0 \qquad \text{(Eq 22)}$$

Which defines that the normal component of the electric field is set to zero.

Transport of diluted species: Diffusion is used as the primary mode of mixing for the fluid

particles. To calculate the time-varying concentration of the dissolved substances in the fluid, the

following convection-diffusion equation is used.

$$\frac{\partial c}{\partial t} + \nabla.(-D\nabla c) = R - u.\nabla c \qquad \text{(Eq 23)}$$

Here, c is defined as the concentration, D is the diffusion coefficient, R is the reaction rate and u

is the flow velocity.

$R = 0$ as there are no reactions that take place in our present study.

At the upper half of the inlet, the concentration is set to C_0. And at the lower half of the inlet, the concentration is set to zero. The solution after mixing flows out from the outlet FG by convection. All other boundaries are set to no flux condition.

4.   **Meshing.** The discretization of the domain is done by creating a mesh in the COMSOL built in mesh builder. The matter of grid generation is a significant consideration in CFD. The generation of an appropriate grid or mesh is one thing, the solution of the governing flow equations over such a grid is quite another thing. Triangular cells were used for this simple 2D geometry because they can be stretched easily to account for different flow gradients in different directions. The cells near the surface have high aspect ratios. For viscous flow through the stenosis, a finely spaced grid was constructed to calculate the details of the flow near the wall. Free triangular cells are used for 2D micromixer meshing. To get better results finer meshing option is used. The number of triangles used is 3012. The number of meshing elements is important to reduce the simulation time and optimization of computational resources. To observe flow properties closely to the electrodes the meshing is done in such a way that the density of the meshing elements is higher than other areas. It is illustrated in figure 44.

For 3D geometry free tetrahedral mesh is used. It is done in the same way as in 2D meshing. The total number of elements is 2395. It is illustrated in figure 45. A normal meshing condition is used to reduce computational time. The density of the meshing elements at the junction is higher than in other areas. Because the change of the flow will occur at the junction point.
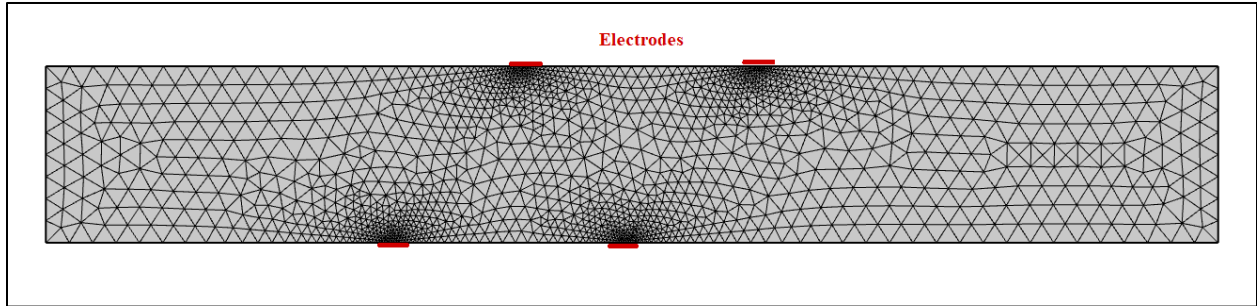
Figure 44: 2D meshing with free triangular cells in 2D micromixer.
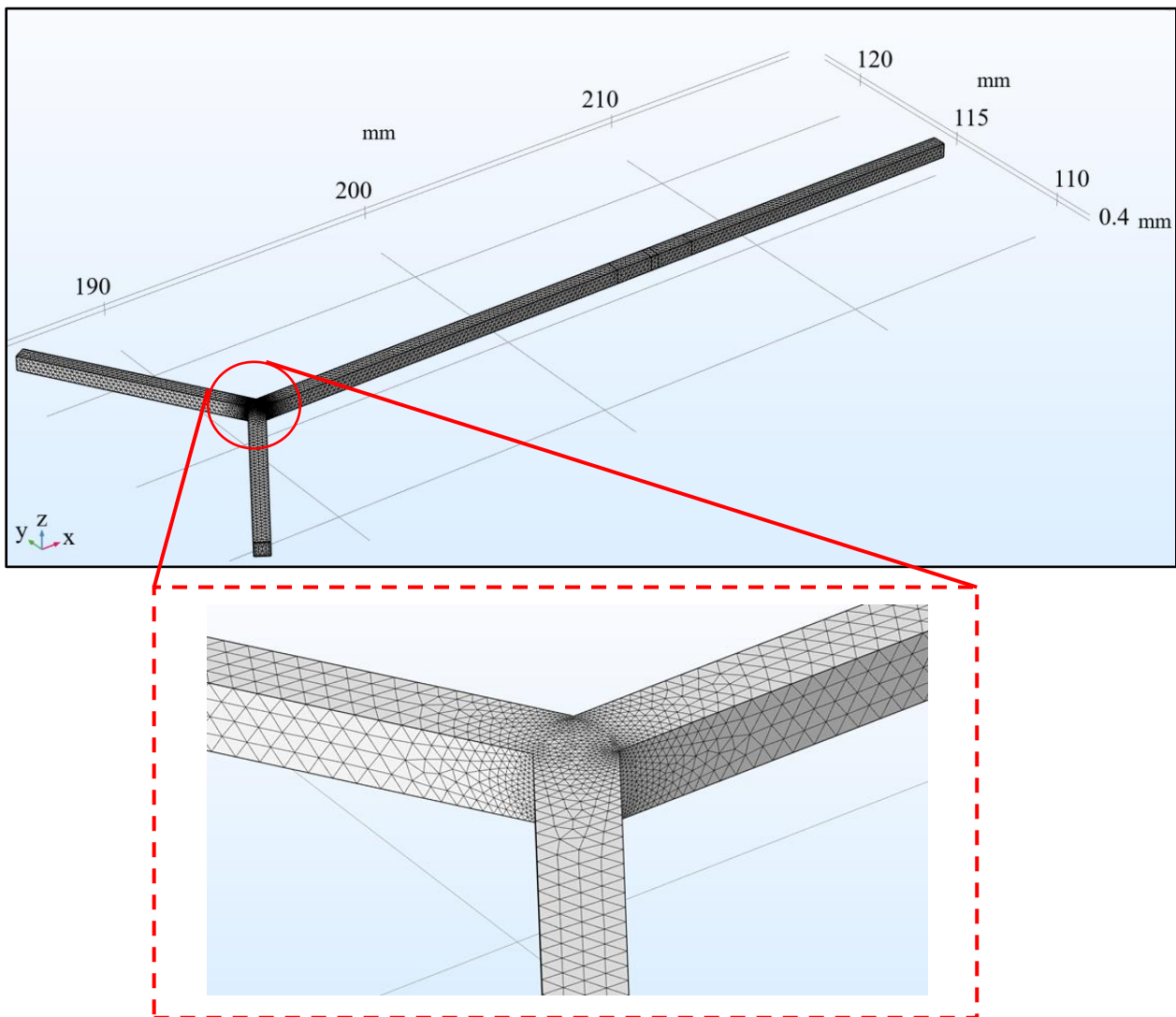
Figure 45: Meshing of the 3D micromixer.

5.   **Solver setting.** A time-dependent electric field is applied to the flowing fluid in a straight microchannel. Along with that concentration gradient flow is applied to know the concentration variation after mixing. So, three parameters (velocity, electric field, and concentration) were solved simultaneously to get the result. Governing equations are solved using the Finite Element Method. To reduce the simulation time and memory requirements, the solution was divided into two stages. First, the amplitude of the electric potential field and the initial state of time-dependent flow was calculated using a stationary solver. Second, the electric current interface was deactivated, and the transient solution was calculated for laminar flow and concentration.

6.   **Result visualization.** Results are evaluated for both 2D and 3D numerical simulations using COMSOL default plotting tools. For velocity and pressure distribution, contour and streamline representation were used. To get concentration and velocity magnitude graph, data from COMSOL simulation was extracted from simulation results. It was exported in Microsoft Excel and then presented in graph format.

CHAPTER VII

NUMERICAL RESULTS

Mesh Independence Test

A free triangular mesh system was used in this study. The mesh system was chosen in a way that can be optimized the computational time and resources as well can give complex insights into the solutions. Concentration distribution was calculated at the channel outlet on three different domain elements. From figure 46, it is found that there are hardly any changes in concentration when domain elements change from 1810 to 4337. So, 1817 was chosen as the optimal domain elements for this work. For the 3D geometry, same procedure has been followed to do the grid independence test.
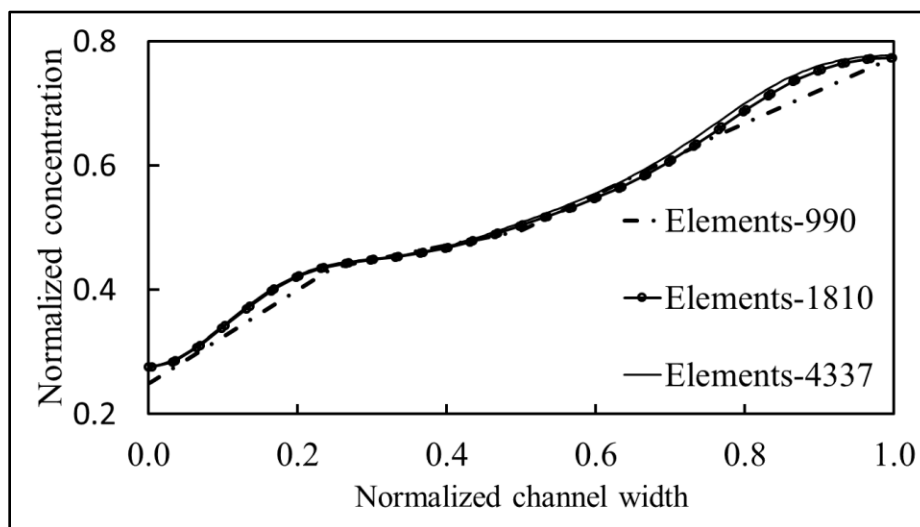

Figure 46: Grid independence test for the normalized concentration at the outlet of the 2D micromixer.

2D active micromixer

An average velocity of 90 µm/s was provided in the inlet of the microchannel. Which leads to a very low Reynold number of 0.0015 flow in the channel. It creates a laminar velocity profile in the channel. In figure 47(b), shows that due to the laminar velocity profile, the concentration of the flow does not change at the outlet of the channel. The high concentration part will mix with a low concentration part only due to the natural diffusion process. It will a long mixing length. For the present case mixing length is only 100 µm. It will require an external force to do the mixing. In figure 47(c), shows that four symmetrical AC voltage was applied in the channel wall. This creates an electroosmotic velocity in the direction of the applied electric field. This disturbs the laminar flow field and creates vortices near the electric field. It forces the high concentration molecules to go to the low concentration region of the channel. In figure 47(c) it is shown that the concentration of the channel becomes closer to 0.5 mol/m^3 at the outlet. It was 1 mol/m^3 at the upper half and 0 mol/m^3 at the lower half of the channel inlet. In figure 47(d), shows the direction and distribution of electric field lines. These field lines are responsible for the complex pattern of fluid streamlines inside the channel when AC electric potential is applied. It is also observed that fluid particles move from positive potential to negative potential. At the location of the first electrode pair BC & KJ, high concentration fluid moves to the direction from BC to KJ. BC is a positive potential source and KJ is a negative potential source. And at the location of DE and IH electrode pair, low concentration fluid moves to the direction from IH to DE. IH is the positive potential and DE is the negative potential source. This model was taken as a base case for the 2D active micromixer model. In the other cases, some parameters like electrodes width, channel width, gap between electrodes were varied in the subsequent experiment.
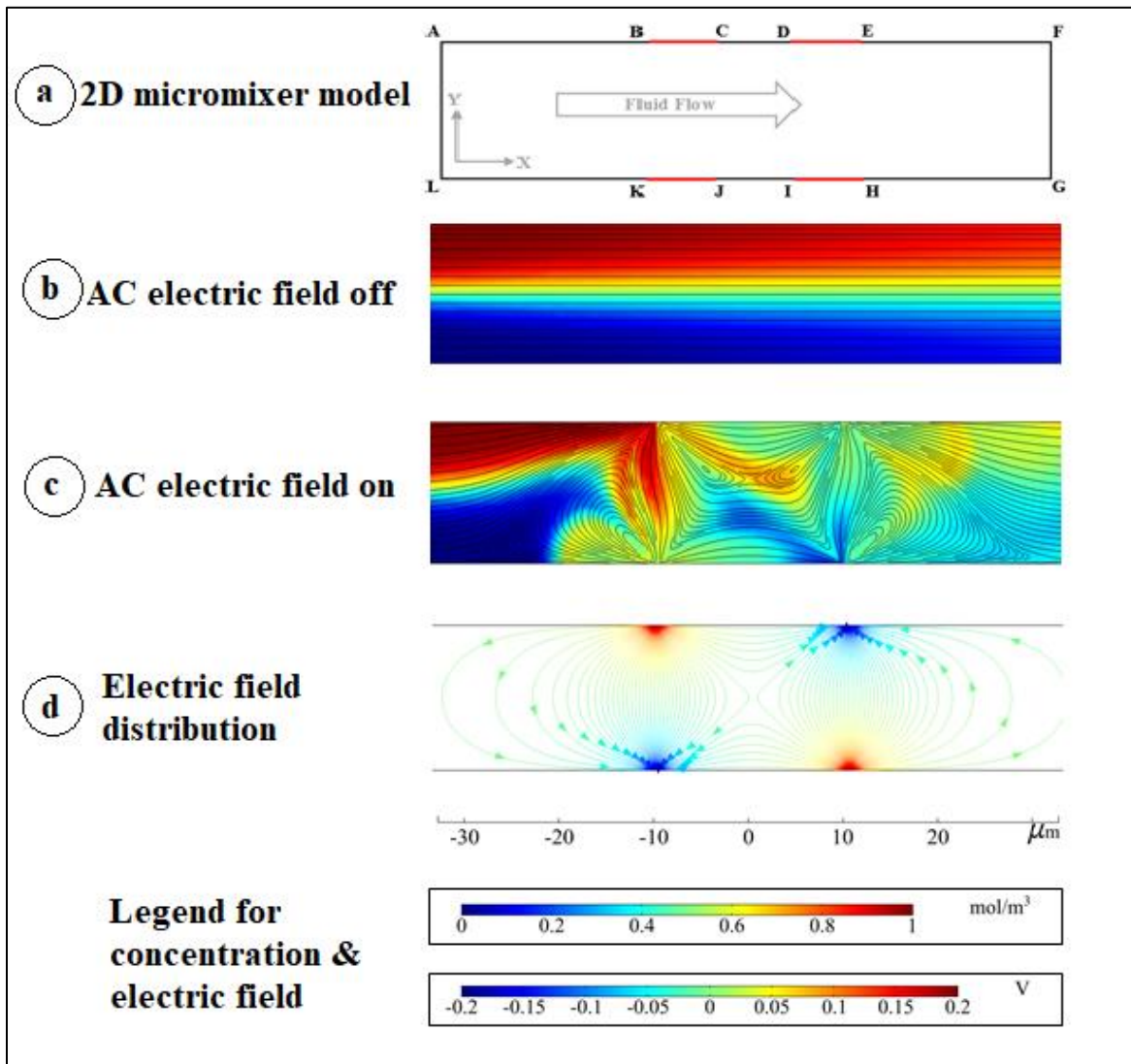
Figure 47: a) 2D active micromixer model, b) surface concentration and velocity streamline in the channel at time t=0.0 s, c) surface concentration, and velocity streamline in the channel at time t=0.475 s, and d) electric field distribution in the channel at time t=0.0 s.

Effect of electrodes spacing

let assume that the distances between the electrodes pair CD & JI are expressed by X. If the value of X is increased keeping all other parameters the same, in figure 48 it is observed that normalized concentration at the outlet moves towards 0.5 up to X=49 µm. It is desired for good

mixing. But if X= 59 µm, then the concentration again moves away from 0.5 at the outlet. For this experiment, the desired normalized concentration at the outlet of the channel is 0.5. It happens because with increasing space between electrodes minimize the effect of electric field on the fluid. So, X= 49 µm is the optimized space between electrodes for this device.
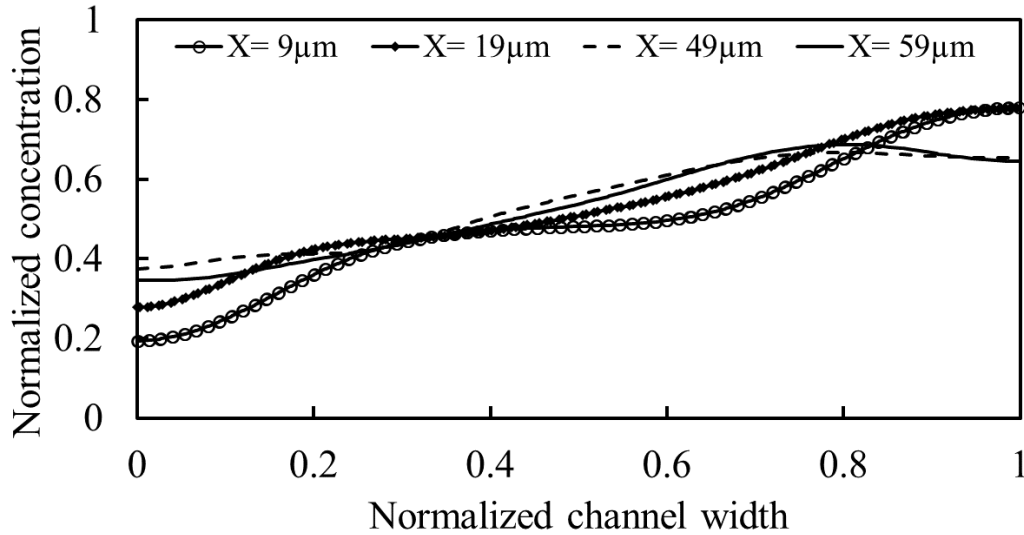
Figure 48: Normalized concentration at the channel outlet with different electrode spacing X.

Effect of channel width

Let us assume that the channel width AL=Y. If Y is increased keeping all other parameters the same, it is observed in figure 49, that the normalized concentration at the channel outlet will be moved further away from the desired concentration at the channel outlet. It is not desirable if we want to increase the channel width. Because fluid particles will not mix-up in this set-up. To solve the problem several simulations were done changing other variables. For this purpose, Y=22.5µm was chosen as the base condition. And the input parameters were changed one by one keeping all other variables constant. It was done to know the contribution of the input parameters to the mixing. First, the magnitude of voltage was increased by two times. In figure

50, it was observed that by doubling the applied voltage, the normalized concentration at the

channel outlet changes significantly from the base condition.
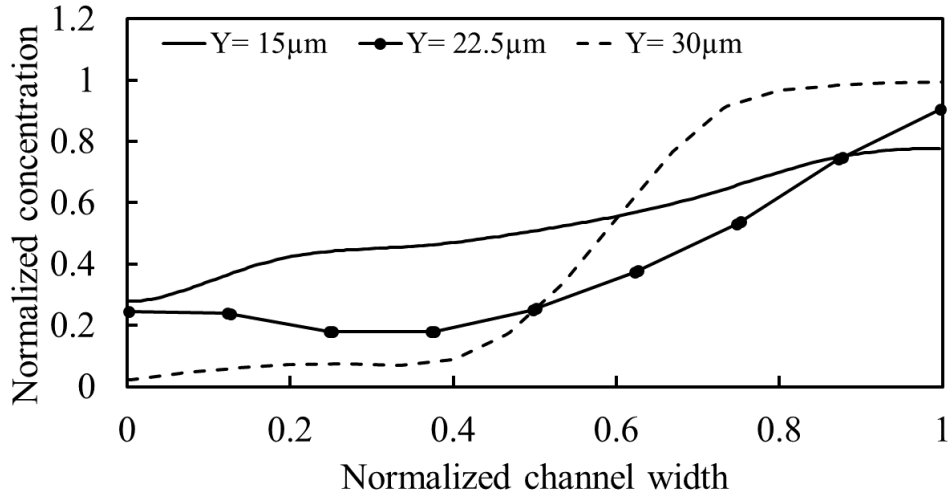
Figure 49: Normalized concentration at the channel outlet with different channel width Y.

The normalized concentration line was moving close to 0.5. It means it offers better mixing than

the base condition while all other variables remain unchanged. Because increasing voltage

magnitude pushes more fluid particles from the upper layer to the lower layer and vice versa.

Second, the frequency was increased by two times from the base condition. It was observed in

figure 50, that the mixing at the channel outlet increases slightly compare to the voltage

magnitude condition. Because the frequency is more related to the inlet velocity of the channel.

Increasing the frequency changes the time scale for the transient time of mixing. Transient time

is defined by the time required for u to reach 95% of the average velocity along channel width.

So, it also depends on the channel width. Third, the length was changed which made them

asymmetric in terms of the arrangements. In figure 50, it is observed that by making the

electrodes asymmetric slightly improve the mixing at the channel outlet compared to the base

condition. Although increasing electrodes length increases the charged surface area which should

increase the number of mixing particles. But with the increased channel width there is not

enough potential available in the electrodes to drive the fluid particles. This is the reason why

mixing isn't improved enough like increasing the voltage magnitude. These results will help us

to determine the input parameters of our desired sized micromixer.
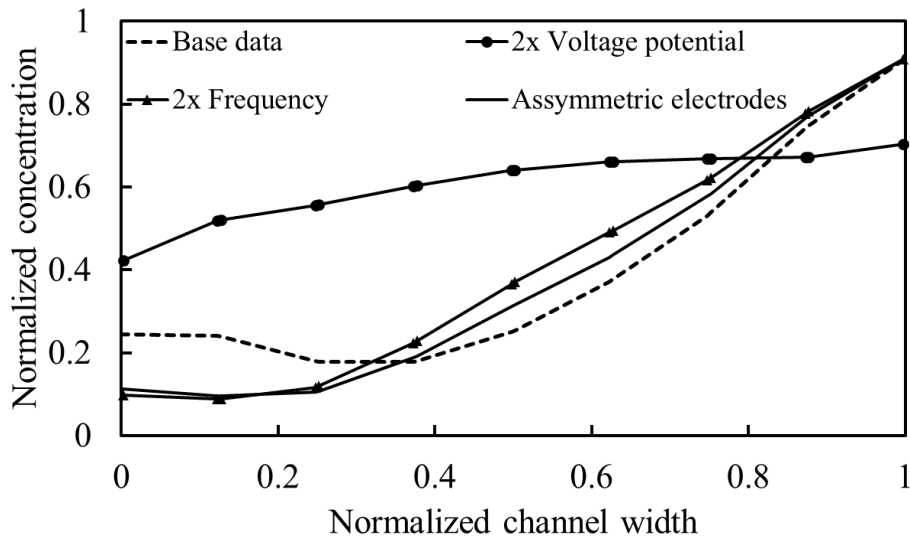
Figure 50: Normalized concentration at the channel outlet with different input conditions.

3D passive micromixer

The concept of designing a device for 3D numerical simulation is quite different from 3D

printing. For 3D printing, the device is designed keeping the fluid occupying part empty. It is

illustrated in figure 51(a). The whole block is solid other than the microchannel part. For

numerical simulation, Only the fluid occupying part is designed. Because only the fluid

movement is going to be observed. So, only the fluidic part of the microchannel is drawn.

Another part of the device is omitted for numerical simulation. It is illustrated in figure 51(b).

The part having used for numerical simulation has the exact dimension as the micromixer

designed for 3D printing. So, the results obtained from numerical simulation can be compared

with the experimental results.
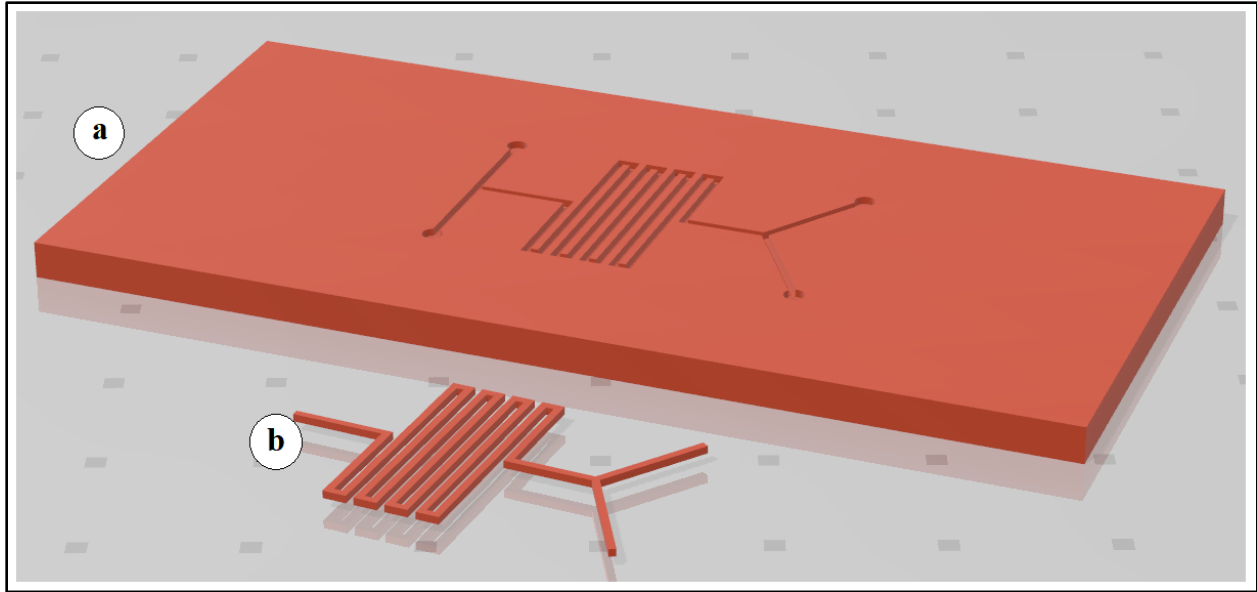
Figure 51: a) 3D view of the micromixer for 3D printing, b) 3D view of the micromixer for 3D simulation.

Concentration distribution inside micromixer

High concentration (1 mol/m^3) fluid passes through one inlet of the micromixer. Low concentration (0 mol/m^3) fluid passes through another inlet of the micromixer. It is illustrated in figure 52. This figure represents the concentration distribution inside the micromixer after giving two different concentration fluid in the inlet. It is observed that after passing through the inlet two different concentration fluid meet with each other in the Y-junction. The two different fluid streams flow side by side without interacting up to bend 1. From bend 1 to bend 2, two fluid streams interact heavily with each other. The two fluid streams continue interacting with each other in the subsequent bend in their way through the outlet. In the outlet, it is observed that the concentration is almost 0.5 mol/m^3. This is the average of the high concentration of 1 mol/m^3 and low concentration 0 mol/m^3. So, it can be said that the two fluids mix with each other completely at the outlet of the micromixer.

68
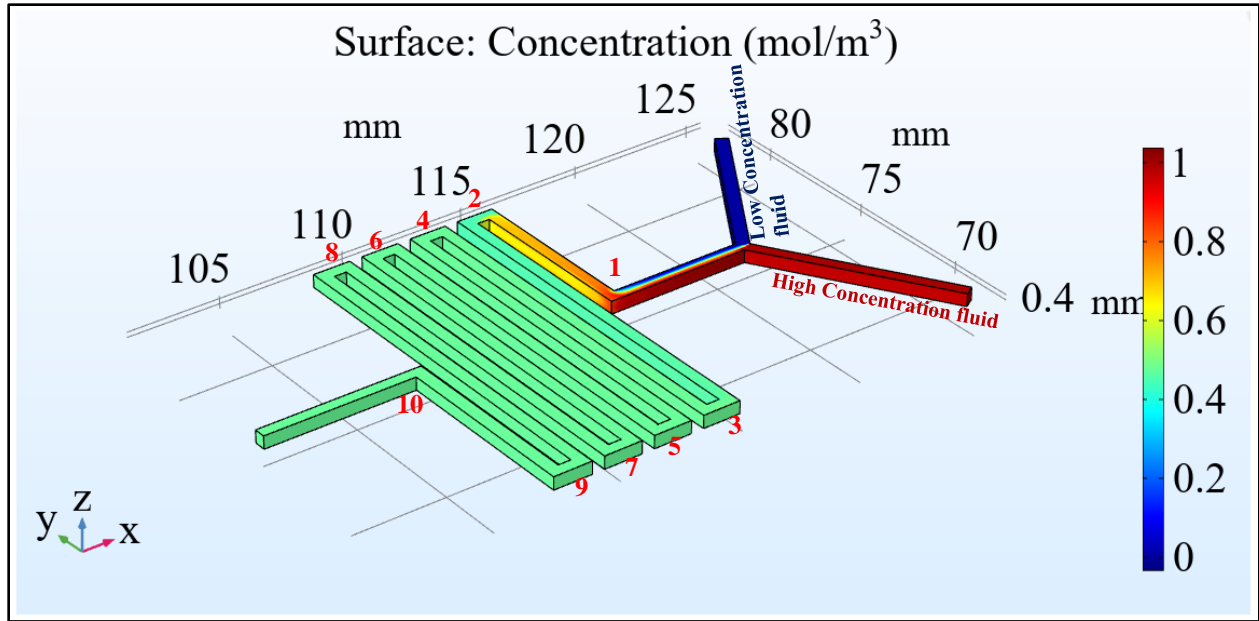
Figure 52: Concentration distribution inside the 3D micromixer.

Flow pattern inside micromixer

To explain the concentration distribution inside the micromixer, flow pattern inside the micromixer is presented in figure 53. Two different concentration fluid mix with each other because of two reasons mainly. One is the natural diffusion occurs between the fluid layers and another one is due to complex flow pattern in the flow path. The flow pattern is responsible to make the diffusion quickly between the two layers. So, if flow pattern changes, the rate of diffusion increases. In the straight microchannel, flow does not change. The mixing in this situation only occurs due to natural diffusion. The flow pattern only changes when there is a bend presents in the flow path. Total 10 bends (figure 52) were designed in this micromixer to change the flow path. When two different concentration fluid meets with each other at Y-junction, they tend to flow separately alongside with each other. It is illustrated in figure 53(b). Fluid streamlines coming from low concentration side remain in this side until bend 1. High concentration fluid lines also remain in the high concentration up to bend 1. Fluid lines from low

concentration side moves to the high concentration in the bend 1. It is illustrated by red dotted

line in figure 53(c). This is where the mixing begins. This also explains the concentration change

in figure 52 immediately after the bend 1. Similar changes also observed in the subsequent bend.

In figure 53(d), it is observed that both low concentration and high concentration fluid lines

changes the sides repeatedly. This increases the diffusion rate. Ultimately, two different

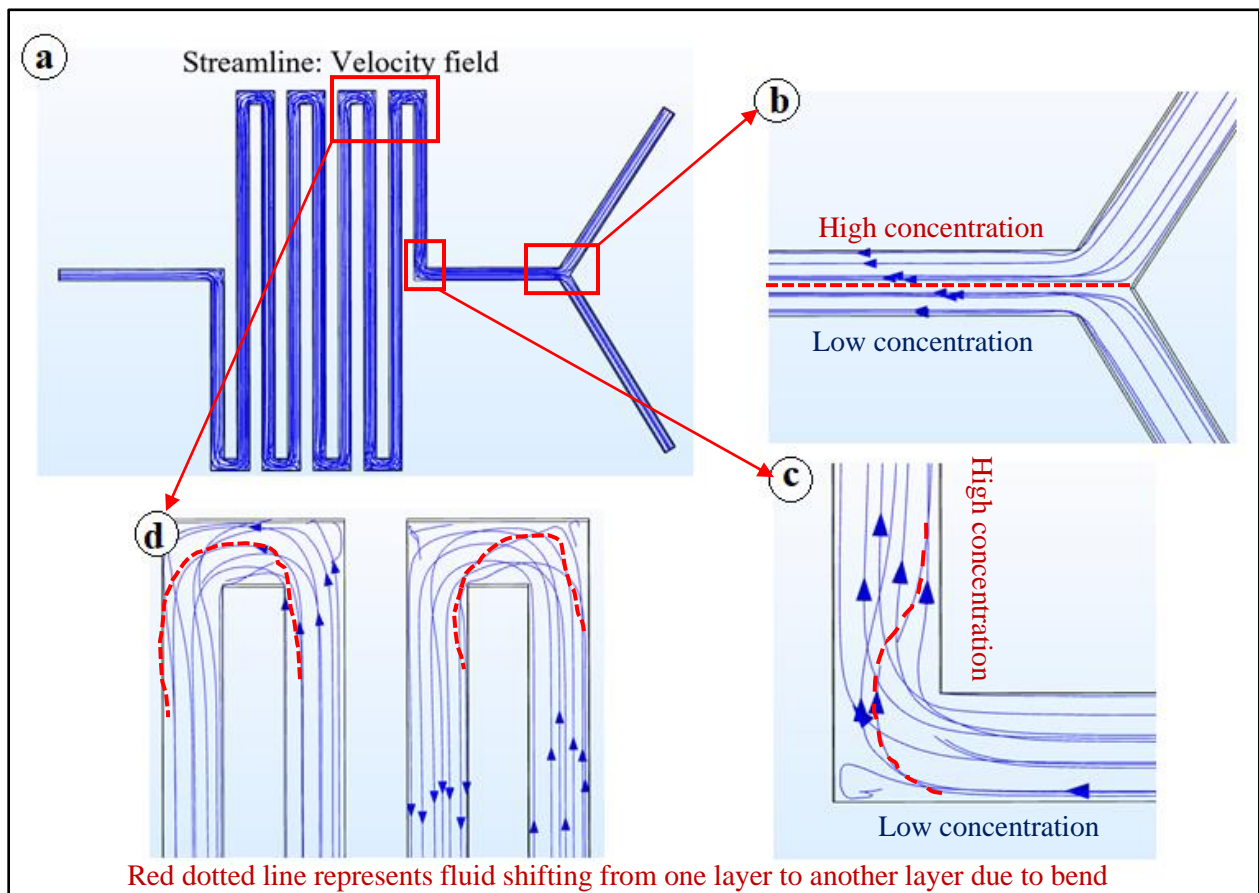concentration fluid mixes with each other at the mixer outlet.

Figure 53: Flow pattern inside the 3D micromixer.

CHAPTER VIII

CONCLUSION

Summary

A micromixer is a crucial part of a lab-on-a-chip device. This lab-on-a-chip device is a game changer for the future health care system in the world. So, the development of micromixer technology can contribute a lot to the future medical diagnostic system by making mixing easier in the microscale for different types of the reagent with the test sample in a lab-on-a-chip device. In this work, two well established micromixer fabrication process were discussed. They are soft lithography and 3D printing microfabrication techniques. These techniques were used to fabricate both active and passive micromixers. The challenges and observations during micromixer fabrication have been highlighted below.

1. Traditional soft lithography is a costly process and requires cleanroom facility. In this work, a low cost optimized soft lithography process is used. It was performed successfully without a cleanroom facility.

2. It is found that a medium resolution (1200 dpi) office printer can be used for mask fabrication. Although a higher resolution printer will give better results.

3. A commercial 365nm UV flashlight (Price. $40) is used as a UV exposure source. It was successfully performed the UV exposure on the SU-8 photoresist.

4. Some cracks were observed at the wall of the micromixer. This problem can be avoided by using a higher resolution printer in the mask fabrication step.

5. By using this optimized soft lithography process, the smallest depth of the microchannel achieved is 40 microns. The smaller can be achieved by changing photoresist model and spin coater set-up.

6. Stereolithography is used in this work as a 3D printing technique. It is very popular in the commercial 3D printing process. But it is not explored much for research purposes. In this work, this printing technique is used in a lab environment to create a microfluidic channel.

7. Unlike the soft lithography process, the 3D printing technique requires only three steps to fabricate a microfluidic device. The fabrication process is very easy compared to the soft lithography process.

8. The 3D printing process took only 25 minutes to fabricate a microfluidic device. On the other hand, it took 150 minutes to fabricate a microfluidic device using soft lithography process.

9. The 3D printing process only requires a printer and photopolymer resins to fabricate a device. The soft lithography technique requires a lot of equipment. So, the total cost of 3D printing is very low compared to soft lithography.

10. The surface finish of a 3D printed device is rough compared to soft lithography fabricated devices. It was also observed that the surface of the soft lithography fabricated device is more hydrophobic than a 3D printed device. So, the soft lithography fabricated device will face less fluidic resistance compared to a 3D printed device.

Although, the 3D printing technique has some advantages over the soft lithography technique as a microfabrication process. But it still has some limitations. Achieving lower dimensions is still a challenge in the 3D printing technique. For the current work, the lowest dimension

achieved using the 3D printing technique is 500 microns. Besides, the 3D printing materials is not transparent compared to PDMS. So, it requires a PDMS layer to observe the flow inside the microfluidic device. These challenges should be explored in the future to use the 3D printing process as a competitive option for microfluidic device fabrication.

The flow dynamics inside the micromixer were observed using the micro-PIV system. The fabricated micromixer was integrated with the micro-PIV system. The syringe pump was used to supply fluid inside the micromixer while the PIV system took photos inside the mixing zone. The flow rate of the syringe pump was 2.00 µl/hr. The observations were summarized below.

1. Fluid layers were observed to be paralleled to each other in the active micromixer, when there was no electricity applied in the electrodes. This parallel fluid layers in the microchannel are called a laminar flow pattern. The mixing between two fluid layers is very unlikely in this case.

2. When electricity was applied in the electrodes of the active micromixer, A sinusoidal flow pattern was observed inside the mixing zone. This sinusoidal flow pattern is responsible to accelerate the diffusion process inside the mixing zone. As a result, a mixed fluid is discharged through the outlet of the active micromixer.

3. An intensified sinusoidal flow pattern was observed inside the micromixer when the voltage and the frequency of electricity is increased. It makes a better mixing environment inside the micromixer.

4. Fluid layers are observed to be paralleled to each other until it reaches to the bend 1 in the passive micromixer. In this region of the micromixer flow pattern is laminar. So, no mixing occurs in this region of the micromixer.

5. Fluid layers inside the micromixer changes direction after passing every bend section. The fluid layers from the lower region move toward the upper region of the channel. This intensified the diffusion process inside the micromixer.

6. These direction changes of the fluid layers occurred repeatedly in the subsequent bend of the passive micromixer. These direction changes contribute to the mixing in the micromixer.

The mixing flow patterns were observed in both active and passive micromixer. The length of the mixing zone in the active micromixer is just 5.00 mm, while the mixing zone in the passive micromixer is 135.00 mm. So, the active micromixer can be used for quick micromixing compared to the passive micromixer. On the contrary, passive micromixer does not require any external force compared to the active micromixer.

COMSOL Multiphysics was used to simulate fluid flow inside both active and passive micromixer to understand the dynamics better inside the mixing zone. The simulation was carried out for both 2D and 3D geometry. The observations are summarized below.

1. The laminar flow profile was found inside 2D active micromixer while electricity was off. The flow pattern was like the flow pattern found in the experimental active micromixer.

2. The complex vortex like flow pattern was observed inside the 2D active micromixer when electricity is on. This complex flow pattern accelerates the mixing inside the active micromixer.

3. The concentration distribution inside the 2D active micromixer shows that the concentration in the upper half of the channel was 1 mol/m^3 at the inlet of the micromixer and 0 mol/m^3 in the lower half of the channel. After mixing It becomes almost 0.5 mol/m^3 at the outlet of the mixer.

4. The flow pattern found in the 3D passive micromixer is analogous to the flow pattern found in the experimental 3D printed passive micromixer.

5. The concentration distribution inside the 3D passive micromixer shows that the high concentration fluid does not mix with low concentration fluid until it passes through bend 1 of the micromixer. The high concentration fluids start mixing with low concentration fluid after passing bend 1. This mixing process continue through the subsequent bend of the micromixer. Finally, a mixed concentration fluid was discharged through the micromixer outlet.

The results observed in the numerical simulation for passive micromixers are analogous to experimental results. However, the numerical flow pattern for active micromixer shows some deviation from the experimental flow pattern. It was occurred due to some dissimilarities (dimensional and geometrical) between the experimental and numerical models of the active micromixer. These observations and results could play an important role in the development of micromixer technology as well as the lab-on -a-chip devices.

Future works

In future, those micromixers have been planned to test in the biological environment. To do that, a bacterial sample will be used to test the micromixer. Already, a bacterial sample was prepared with the support of the biology department. The sample preparation steps are illustrated in figure 54. Listeria Innocua bacteria sample is prepared and ready to use. It is a food born pathogen. The effect of different sanitizer will be tested on these bacteria in a microfluidic environment. The sanitizer solutions will be mixed with the bacteria sample in the micromixer.
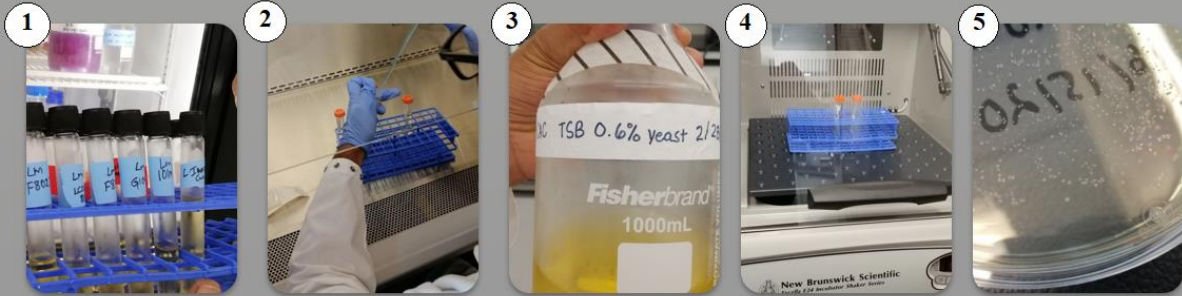
Figure 54: Bacterial sample preparation steps.

REFERENCES

[1] Castillo-Leon, Jaime & Svendsen, Winnie & Dimaki, Maria & Arima, Valentina & Akram, Muhammad & Miserere, Sandrine & Neumann, Christiane & Kipling, G. (2015). Lab-on-a-Chip Devices and Micro-Total Analysis Systems A Practical Guide. 10.1007/978-3-319-08687-3.

[2] Chen, H., Zhang, Y.T., Mezic, I., Meinhart, C.D. and Petzold, L., "Numerical simulation of an electroosmotic micromixer", Proceedings of Microfluidics 2003, ASME IMECE, Washington DC, November 2003.

[3] He B, Burke B, Zhang X, Zhang R, Regnier F (2001) A picoliter-volume mixer for microfluidic analytical systems. Anal Chem 73(9):1942–1947.

[4] Zhong, Shao-Long; Dang, Zhi-Min; Zhou, Wen-Ying; Cai, Hui-Wu: 'Past and future on nanodielectrics', IET Nanodielectrics, 2018, 1, (1), p. 41-47, DOI: 10.1049/iet-nde.2018.0004.

[5] Hong, C., Choi J., and Ahn C. H., 2004, "A Novel in-plane Passive Microfluidic Mixer with Modified Tesla Structures," Lab Chip, 4, pp. 109-113.

[6] Wu, J., 2008, "Interactions of Electrical Fields with Fluids: Laboratory-on-a-chip Applications," *IET Nanobiotechnology*, 2(1), pp. 14-27.

[7] Chen, H., Zhang, Y. T., Mezic, I., Meinhart, C. D. and Petzold, L., "Numerical Simulation of an Electroosmotic Micromixer," Proc. ASME International Mechanical Engineering Congress and Exposition, IMECE2003-55017, pp. 653-658, Washington, D.C., November 15-21, 2003.

[8] Hadigol, M., Nosrati, R., Nourbakhsh, A. and Raisee, M., 2011, "Numerical Study of Electroosmotic Micromixing of non-Newtonian Fluids," Journal of Non-Newtonian Fluid Mechanics, 166, pp. 965-971.

[9] Zhang, Y. T., Chen, H., Mezic, I., Meinhart, C. D., Petzold, L. and MacDonald, N. C., 2004, "SOI Processing of a Ring Electrokinetic Chaotic Micromixer," NSTI-Nanotech, 1, pp. 292-295.

[10] Sasaki, N., Kitamori, T. and Kim, H. B., 2006, "AC Electroosmotic Micromixer for Chemical Processing in a Microchannel," Lab on a Chip, 6, pp. 550-554.

[11] Ahmed, F. and Kim, K. Y., 2017, "Parametric Study of an Electroosmotic Micromixer with Heterogeneous Charged Surface Patches," Micromachines, 8 (7), 199.

[12] Zhou, T., Wang H., Shi, L., Liu, Z. and Joo, S. W., 2016, "An Enhanced Electroosmotic Micromixer with an Efficient Asymmetric Lateral Structure," Micromachines, 7, 218.

[13] Zhang, K., Ren, Y., Hou, L., Feng, X., Chen, X. and Jiang, H., 2018, "An Efficient Micromixer Actuated by Induced-Charge Electroosmosis Using Asymmetrical Floating Electrodes," Microfluid Nanofluid, 22, 130, doi:10.1007/s10404-018-2153-2.

[14] Usefian, A. and Bayareh, M., 2019, "Numerical and Experimental Study on Mixing Performance of a Novel Electro-osmotic Micromixer," M. Meccanica, 54:1149, doi: 10.1007/s11012-019-01018-y.

[15] Yang K., Islam N., Eda S., and Wu J., "Optimization of an AC Electrokinetics immunoassay lab-chip for biomedical diagnostics," Microfluid Nanofluid, 2017, Vol. 21, No. 35.

[16] Medoro G., Manaresi N., Leonardi A., Altomare L., Tartagni M., and Guerrieri R., "A Lab-on-a-chip for cell detection and manipulation," IEEE Sensors Journal, 2003, Vol. 3, No. 3.

[17] Wu J., Ben Y., Battigelli D., and Chang H., "Long-range AC electroosmotic trapping and detection of bioparticles," Industrial & Engineering Chemistry Research, 2005, 44(8), pp. 2815-2822.

[18] Tomkins M.R., Chow J., Lai Y., and Docoslis A., "A coupled cantilever-microelectrode biosensor for enhanced pathogen detection," Sensors and Actuators B, 2013, 176, pp. 248-252.

[19] Song Y., Chen P., Chung M.T., Nidetz R., Park Y., Liu Z., McHugh W., Cornell T.T., Fu J., and Kurabayashi K., "AC electroosmosis-enhanced nanoplasmofluidic detection of ultralow-concentration cytokine," Nano Letter, 2017, 17, pp. 2374-2380.

[20] FORMLABS white paper: Intro to Stereolithography 3D Printing (https://formlabs.com/blog/introduction-to-stereolithography/)

BIOGRAPHICAL SKETCH

Md Fazlay Rubby was born in Rangpur, Bangladesh in 1991. Most of his life was spent on dreaming and developing a fascination for technology and engineering. Md Fazlay Rubby received his Bachelor's in mechanical engineering from the Bangladesh University of Engineering and Technology in 2014 and his Master's in electrical engineering from the University of Texas Rio Grande Valley in 2020. While pursuing his master's degree, he has presented research work in several conferences organized by the fluid engineering division of American Society of Mechanical Engineers (ASME). He also reviewed many conference and journal papers. For his contributions in fluid dynamics and microfluidics, he was awarded as a Graduate Student Scholar (GSS) from fluid engineering division of ASME. His main research interest is to fabricate microfluidic devices (mixers, pumps, manipulator, etc.) and analysis of flow dynamics inside those devices for Lab-on-a-Chip and Point-of-care-testing diagnostics applications. Upon graduation from the University of Texas Rio Grande Valley, Md Fazlay Rubby is looking forward to beginning PhD program in the United States.

Permanent address: Dewantulli, Mahigonj, Rangpur-5403, Bangladesh.

Permanent email address: fazlay.rubby61@gmail.com